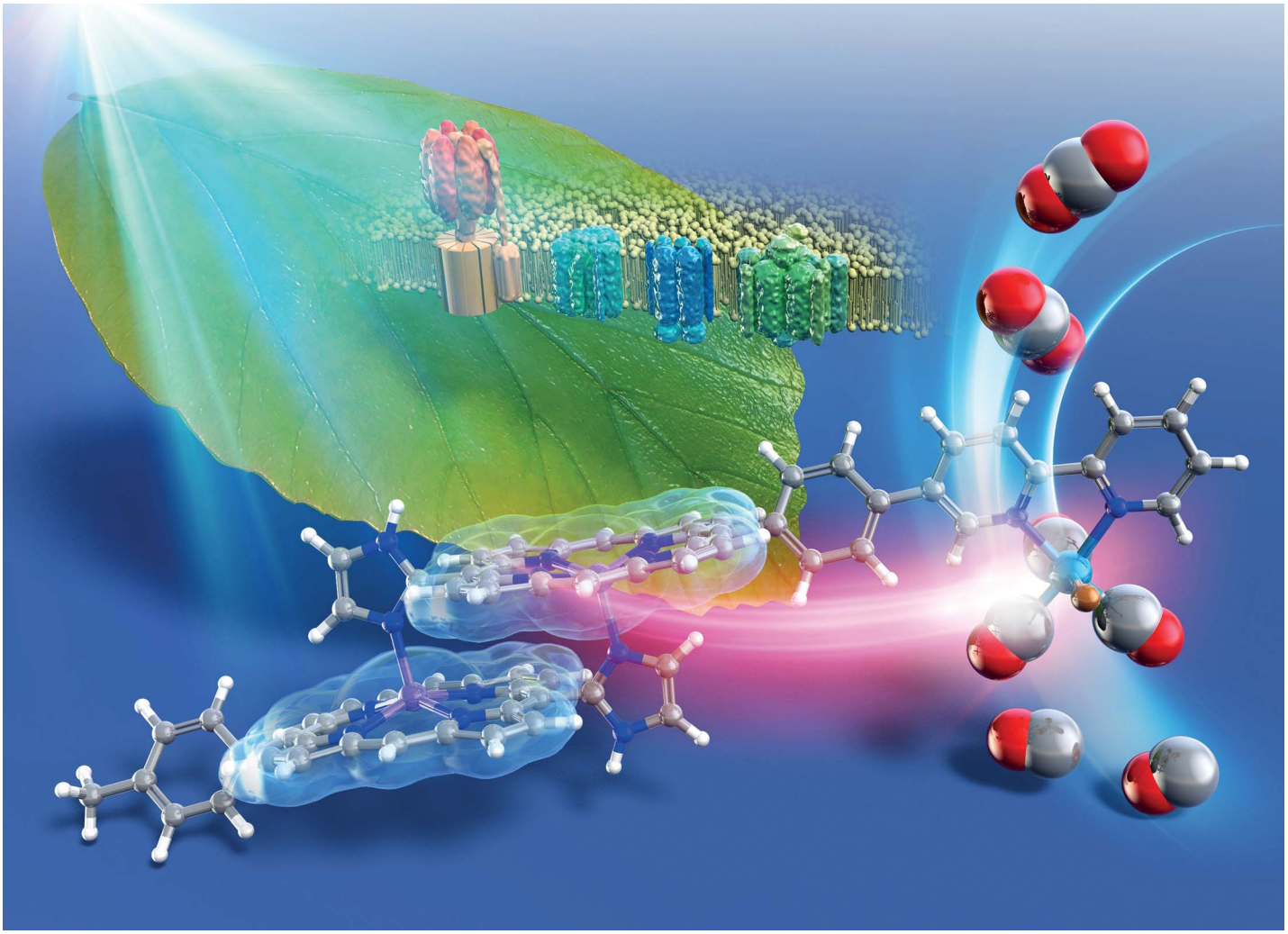

Showcasing research from Kuramochi's group in Prof. Satake's laboratory, Tokyo University of Science, Japan.

Photocatalytic CO_2 reduction sensitized by a special-pair mimic porphyrin connected with a rhenium(I) tricarbonyl complex

Zn porphyrins with an imidazolyl group at the *meso* position generate a highly stable porphyrin dimer by complementary coordination from the imidazolyl to the Zn ion, which mimics the natural special pair in photosynthesis. In this work, we have synthesized an imidazolyl-substituted Zn porphyrin connected with a Re 2,2-bipyridine tricarbonyl complex as a CO_2 reduction catalyst. The porphyrin dimer acted as a good photosensitizer in photocatalytic CO_2 reduction, giving CO with high selectivity and durability.

As featured in:

See Yusuke Kuramochi, Akiharu Satake *et al.*, *Chem. Sci.*, 2022, **13**, 9861.

ROYAL SOCIETY OF CHEMISTRY

rsc.li/chemical-science

Registered charity number: 207890

Chemical Science

ROYAL SOCIETY OF CHEMISTRY

EDGE ARTICLE

View Article Online
View Journal | View Issue

Check for updates

Cite this: *Chem. Sci.*, 2022, **13**, 9861

All publication charges for this article have been paid for by the Royal Society of Chemistry

Open Access Article. Published on 03 augusta 2022. Downloaded on 20.10.2025 1:09:44.
This article is licensed under a Creative Commons Attribution-NonCommercial 3.0 Unported Licence.

Photocatalytic CO_2 reduction sensitized by a special-pair mimic porphyrin connected with a rhenium(I) tricarbonyl complex†

Yusuke Kuramochi, *[ab] Ren Sato,[a] Hiroki Sakuma[b] and Akiharu Satake *[ab]

Zn porphyrins with an imidazolyl group at the *meso* position generate a highly stable porphyrin dimer by complementary coordination from the imidazolyl to the Zn ion in noncoordinating solvents such as chloroform, which mimics the natural special pair in photosynthesis. In this work, we have synthesized an imidazolyl-substituted Zn porphyrin connected with a Re 2,2-bipyridine tricarbonyl complex as a CO_2 reduction catalyst *via* a *p*-phenylene linker, affording a homodimer with two Re complexes on both sides (**ReDRe**). The dimeric structure is easily dissociated into the corresponding monomers in coordinating solvents. Therefore, we prepared a mixture containing a heterodimer with the Re carbonyl complex on one side (**ReD**) by simple mixing with an imidazolyl Zn porphyrin and evaporating the solvent. Using the Grubbs catalyst, the subsequent olefin metathesis reaction of the mixture gave covalently linked porphyrin dimers through the allyloxy side chains, enabling the isolation of the stable hetero- (**ReD′**) and homo-dimers (**ReD′Re**) with gel permeation chromatography. The Zn porphyrin dimers have intense absorption bands in the visible light region and acted as good photosensitizers in photocatalytic CO_2 reduction in a mixture of *N*,*N*-dimethylacetamide and triethanolamine (5 : 1 v/v) containing 1,3-dimethyl-2-phenyl-2,3-dihydro-*1H*-benzo[*d*]imidazole as the electron donor, giving CO with high selectivity and durability. Under irradiation with strong light intensity, the reaction rate in **ReD′** exceeded that of the previous porphyrin=Re complex dyad, **ZnP-phen=Re**. For instance, after irradiation at 560 nm for 18 h, the turnover number (TON_{CO}) of **ReD′** reached 2800, whereas the TON_{CO} of **ZnP-phen=Re** was 170. The high activity in the system using the porphyrin dimer originates from no accumulation of the one-electron reduced species of the porphyrin that inhibit light absorption due to the inner-filter effect.

Received 10th June 2022
Accepted 27th July 2022

DOI: 10.1039/d2sc03251a

rsc.li/chemical-science

Introduction

Undoubtedly, CO_2 emissions caused by human activity have drastically changed the global climate. Various systems have been developed to reduce CO_2 in the atmosphere, and systems converting CO_2 into energy-rich compounds with the aid of light (solar energy) have much potential to solve not only the problem of global warming, but simultaneously also that of a shortage of fossil-fuel resources.[1] Sunlight consists mainly of visible light with low photon density. The low photon density can be disadvantageous, in particular in multielectron reactions, and therefore photosensitizers capturing visible light with high efficiency are essential.[2] In natural photosynthesis, dilute sunlight is collected by networks of pigments—the so-called light-harvesting complexes.[3] The collected energy is transferred to the chlorophyll dimer in the reaction center, the so-called "special pair", that initiates photoinduced electron transfer to give a charge-separated (CS) state in the reaction center.[4]

In 1994, Kobuke *et al.* reported that Zn porphyrins having an imidazolyl group at the *meso* position form a slipped-cofacial dimeric structure by complementary coordination from the imidazolyl to the Zn ion of the porphyrin center in non-coordinating solvents, and that the dimeric structure mimics the special pair in photosynthetic systems.[5] When the dimer is one-electron oxidized, the produced radical cation delocalizes over two porphyrin units. The CS rate is accelerated in the photoinduced electron transfer, while the charge-recombination rate decelerates to give the ground state.[6] The dimeric structure is sufficiently stable to be treated as a photosensitizer in noncoordinating solvents such as chloroform and toluene, but it easily dissociates into monomeric units in coordinating solvents such as pyridine and dimethyl sulfoxide (DMSO). These properties are somewhat advantageous for preparing various combinations of dimers.[7] The porphyrin

[a]*Graduate School of Science, Tokyo University of Science, 1-3 Kagurazaka, Shinjuku-ku, Tokyo, 162-8621, Japan*

[b]*Department of Chemistry, Faculty of Science Division II, Tokyo University of Science, Japan. E-mail: kuramochiy@rs.tus.ac.jp; asatake@rs.tus.ac.jp*

† Electronic supplementary information (ESI) available: Synthetic procedures, NMR, MALDI-TOF mass, IR, UV-vis and fluorescence spectra, GPC-HPLC charts, calculations for fluorescence quenching experiments, CV, DPV, energy diagrams, and photocatalytic CO_2 reduction. See https://doi.org/10.1039/d2sc03251a

© 2022 The Author(s). Published by the Royal Society of Chemistry

Open Access Article. Published on 03 augusta 2022. Downloaded on 20.10.2025 1:09:44.
This article is licensed under a Creative Commons Attribution-NonCommercial 3.0 Unported Licence.

units can be freely exchanged by simply mixing two porphyrin components in a coordinating solvent followed by evaporating the solvent, giving a hetero-porphyrin dimer. For instance, a triad system consisting of a porphyrin dimer with ferrocene as an electron donor on the one side and fullerene as an electron acceptor on the other side was easily formed by the simple mixing of two kinds of Zn porphyrin having either ferrocene or fullerene. The supramolecular triad gave long-lived CS species after efficient photoinduced electron transfer and charge shift.[8] In addition, this dimer-based supramolecular methodology is applicable in the construction of various self-assembled porphyrin arrays having cyclic, chain, and sheet structures for photosynthetic antenna models,[9–11] two-photon absorption materials,[12] solar cell materials,[13] solvation/desolvation indicators,[14] and so on.

Zn porphyrin has been used as the photosensitizer in homogeneous photoredox reactions.[15,16] For example, dyads combining Zn porphyrin and the Re diimine tricarbonyl complex catalyst have been developed for photocatalytic CO_2 reduction.[16–18] Among them, we have recently reported on a Zn porphyrin=Re complex dyad, **ZnP-phen=Re** (Fig. 1), in which *fac*-Re(phen)$(CO)_3$Br (where phen = 1,10-phenanthroline) is connected with a Zn porphyrin, and affords CO with high selectivity (>99.9%) and efficiency (Φ_{CO} = 8% and turnover number (TON_{CO}) > 1300) in photocatalytic CO_2 reduction using 1,3-dimethyl-2-phenyl-2,3-dihydro-1*H*-benzo[*d*]imidazole (BIH) as an electron donor, phenol as a proton source, and *N*,*N*-dimethylacetamide (DMA) as a solvent.[18]

In this work, Kobuke's special-pair mimic porphyrin was first used as the photosensitizer for photocatalytic CO_2 reduction. It is expected that the slipped-cofacial dimer has the advantage that the dimer can utilize light of a wider wavelength because the intense Soret band appearing at ~420 nm of monomeric porphyrin is split by strong excitonic coupling between two Zn porphyrins in close proximity.[19] In addition, because the dimeric structure can be easily dissociated in coordinating solvents, unsymmetric heterodimers can be constructed by simply mixing two kinds of porphyrin in a coordinating solvent and then evaporating the solvent. Furthermore, a multisite ring-closing metathesis reaction using the Grubbs catalyst on olefin moieties at the *meso* positions of the porphyrin fixes the dimeric structure through covalent bonds, giving a stable dimer that does not dissociate even in coordinating solvents such as pyridine or DMSO.[20] We have synthesized a Re bipyridine tricarbonyl complex connected to the opposite *meso* position of the imidazolyl Zn porphyrin through a *p*-phenylene linker. The porphyrin forms a stable dimer having the Re complex on both sides (**ReDRe**). The reorganizing procedure by mixing **ReDRe** and a dimer without the Re complex (**D**) in pyridine and evaporating the solvent gave a mixture of **ReDRe**, **D**, and a hetero-dimer having the Re complex on one side (**ReD**). The ring-closing metathesis reaction followed by separation of the mixture with gel permeation chromatography (GPC) produced covalently linked dimers, **ReD′** and **ReD′Re** (Fig. 1). Here, a bulky isostearyl group (IS group) was introduced on the imidazolyl group in **ReDRe** to be soluble in practical organic solvents. The photocatalytic reaction in CO_2-saturated DMA containing BIH showed that the triethanolamine (TEOA) presence dramatically improved the catalytic activity. In addition, we performed photocatalytic CO_2 reduction using **ReDRe** and **ReD′Re** in DMSO, and **ReD′Re** had higher durability than **ReDRe**, which was dissociated to the monomers in DMSO, demonstrating that the dimeric structure plays an important role for the high activity in photocatalytic reactions.

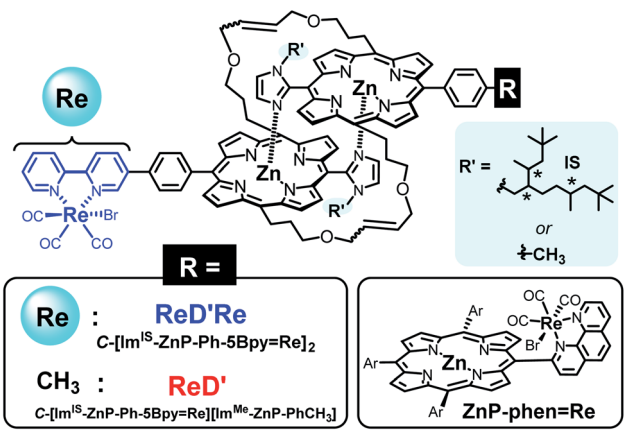

Fig. 1 Structures of the porphyrin dimers having the Re complex(es) (ReD′Re and ReD′) and the porphyrin=Re complex dyad (ZnP-phen=Re). The asterisks in the IS group indicate asymmetric carbons.

Results and discussion

Synthesis of ReDRe

First, we attempted to synthesize the porphyrin dimer having 1-methyl-imidazolyl groups at the *meso* positions of the porphyrins (see the ESI†). However, when the Re tricarbonyl complexes were introduced into the bpy groups of **[Im^{Me}-ZnP-Ph-5Bpy]$_2$**, the product became insoluble in preferred solvents (chloroform, dichloromethane, toluene, and acetonitrile) for the ring-closing metathesis reaction using the Grubbs catalyst as the dimer. **[Im^{Me}-ZnP-Ph-5Bpy=Re]$_2$** was soluble in *N*,*N*-dimethylformamide (DMF) and the ^{1}H NMR spectrum recorded under high-concentration conditions showed an almost dimeric structure in DMF-d_7 (Fig. S14†). However, **[Im^{Me}-ZnP-Ph-5Bpy=Re]$_2$** was partially dissociated intothe monomer in the concentration range for the intramolecular metathesis reaction of the dimer. We also tried the ring-closing metathesis reaction with the dimer, **[Im^{Me}-ZnP-Ph-5Bpy]$_2$**, before the introduction of the Re complex, but the reaction did not proceed, probably due to the deactivation of the Grubbs catalyst (1st generation) by coordination of the bpy groups.[21] Therefore, we changed the substituent group on the imidazolyl moiety from the methyl group to a bulky IS group (Fig. 1) to improve organic solvent solubility. Scheme 1 shows the synthetic route for the porphyrin dimer having the IS groups at the imidazolyl groups and Re tricarbonyl complexes at the bpy groups (**[Im^{IS}-ZnP-Ph-5Bpy=Re]$_2$**, **ReDRe**). The free-base porphyrin **Im^{IS}-H$_2$P-PhI** was synthesized with 19% yield by condensation of 4-iodobenzaldehyde and **Im^{IS}-CHO** with *meso*-(3-allyloxypropyl)dipyrromethane at room temperature (rt). The three asymmetric C

© 2022 The Author(s). Published by the Royal Society of Chemistry

Open Access Article. Published on 03 augusta 2022. Downloaded on 20.10.2025 1:09:44.
This article is licensed under a Creative Commons Attribution-NonCommercial 3.0 Unported Licence.

atoms of the IS groups provide $2^3 = 8$ stereoisomers and their conformational isomers, resulting in broadened and complicated signals in their ^{1}H and ^{13}C NMR spectra. Successful syntheses of the porphyrins were confirmed by not only using 2-dimensional (2D) NMR but also by comparing with the spectra of porphyrins substituted by 1-methyl-imidazolyl. The complicated signals appearing from 1.38 to −0.80 ppm in the ^{1}H NMR spectrum of **Im^{IS}-H$_2$P-PhI** were assigned to the methine, methylene, and methyl signals of the IS groups (Fig. S36†). The Zn(II) ion was introduced into **Im^{IS}-H$_2$P-PhI** by treatment with a methanol solution of $Zn(OAc)_2$ in $CHCl_3$. The ^{1}H NMR spectrum showed that the *Im*-4 and *Im*-5 protons that appeared at 7.74–7.72 ppm and 7.52–7.50 ppm in **Im^{IS}-H$_2$P-PhI** were shifted to a higher field by the Zn insertion to show the peaks at 2.06 ppm for the *Im*-4 proton and at 5.56 ppm for the *Im*-5 proton. The spectral change was similar to that of **[Im^{Me}-ZnP-PhI]$_2$**, indicating that all the stereoisomers quantitatively construct the slipped-cofacial dimer, **[Im^{IS}-ZnP-PhI]$_2$** (Fig. S42†). The dimeric structure was also clarified by the characteristic split Soret band in the ultraviolet visible (UV-vis) absorption spectrum (Fig. S46†).[19]

The porphyrin dimer with the bpy groups, **[Im^{IS}-ZnP-Ph-5Bpy]$_2$**, was synthesized by the Suzuki–Miyaura coupling reaction of **[Im^{IS}-ZnP-PhI]$_2$** and 5-(4,4,5,5-tetramethyl-1,3,2-dioxaborolan-2-yl)-2,2′-bipyridine (**5Bpy-B(OR)$_2$**) in toluene and DMF. The reaction was first performed under anhydrous conditions, but the coupling reaction did not proceed. The coupling reaction proceeded with water addition, giving **[Im^{IS}-ZnP-Ph-5Bpy]$_2$** at 89% yield. The product, **[Im^{IS}-ZnP-Ph-5Bpy]$_2$**, also showed the split Soret bands in the UV-vis absorption spectrum and the upper-field shifts of the β-pyrrole and imidazolyl protons compared with the free-base porphyrin in the ^{1}H NMR spectrum (Fig. S48†), indicating that the bpy group does not interrupt the formation of the dimeric structure. Here, **5Bpy-B(OR)$_2$** was difficult to purify with column-chromatographic techniques due to the decomposition of boron derivatives on the silica gel column.[22] Thus, **5Bpy-B(OR)$_2$** was purified by partitioning between the aqueous and organic layers. The lithiation of 5-bromo-2,2′-bipyridine followed by addition of triisopropyl

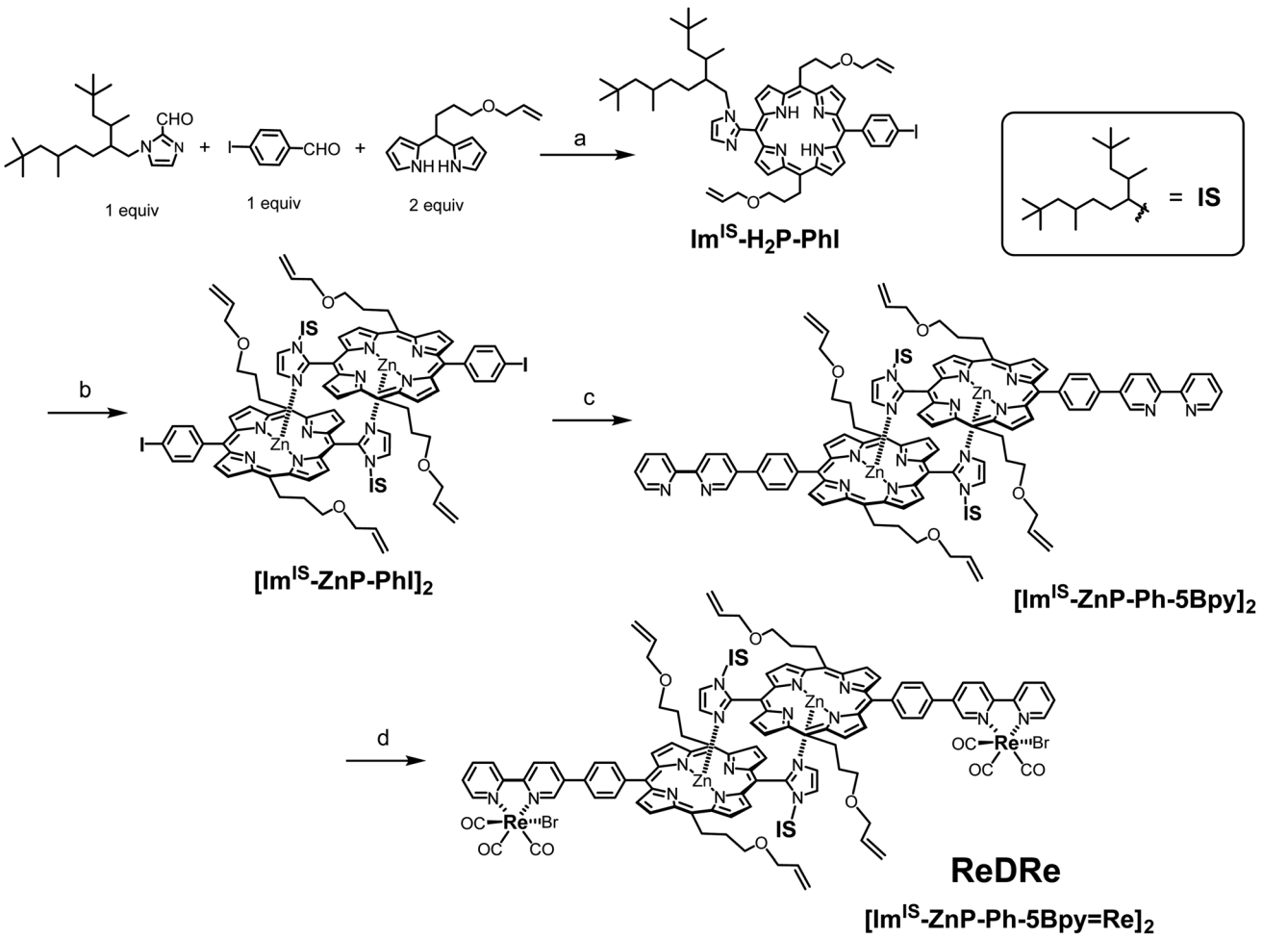

Scheme 1 Synthetic route of the noncovalently linked porphyrin dimer, [Im^{IS}-ZnP-Ph-5Bpy=Re]$_2$ (ReDRe). Reagents and conditions: (a) (i) trifluoroacetic acid/$CHCl_3$, rt, and 3.5 h, (ii) Et_3N, *p*-chloranil, rt, overnight, and 19%; (b) $Zn(OAc)_2$ (8 equivalent (equiv.)), $CHCl_3$/CH_3OH, rt, overnight, and 96%; (c) 5-(4,4,5,5-tetramethyl-1,3,2-dioxaborolan-2-yl)-2,2′-bipyridine (5Bpy-B(OR)$_2$, 1.5 equiv.), $Pd(PPh_3)_4$ (0.2 equiv.), $CsCO_3$ (2.9 equiv.), toluene/DMF/water, 90 °C, 4 h, and 89%; (d) $Re(CO)_5Br$ (0.97 equiv.), toluene, 90 °C, 2 d, and 72%.

Open Access Article. Published on 03 augusta 2022. Downloaded on 20.10.2025 1:09:44.
This article is licensed under a Creative Commons Attribution-NonCommercial 3.0 Unported Licence.

borate gave a boronic acid derivative, which was extracted at pH = 11 to the aqueous layer to remove the starting material and by-products existing the organic layer. Next, the aqueous layer was evaporated to dryness, and the residue was reacted with pinacol. Pure **5Bpy-B(OR)$_2$** was extracted with toluene and other impurities remained as insoluble materials (see the ESI†).

The introduction of the Re(I) tricarbonyl complex into the bpy groups of **[Im^{IS}-ZnP-Ph-5Bpy]$_2$** was performed by refluxing with $Re(CO)_5Br$ in toluene. The use of excess amounts (1.5 equiv.) of $Re(CO)_5Br$ against the bpy group made the characteristic split Soret band of the dimeric structure change into a single Soret band (Fig. S55†). This observation indicates that the coordination of the excess Re(I) ion to the imidazolyl group of the porphyrin dissociates the dimer to give a monomeric species. The reflux of the mixture in pyridine recovered the split Soret band and gave the target compound, **[Im^{IS}-ZnP-Ph-5Bpy=Re]$_2$** (**ReDRe**, Fig. S55 and 56†), indicating that the monodentate imidazole Re complex dissociated in pyridine, whereas the bidentate bpy complex was stable in pyridine even under reflux conditions. The use of 0.97 equiv. of $Re(CO)_5Br$ selectively gave the target compound without forming the monomeric species, (Fig. S55†), and the purification on a silica gel column afforded **ReDRe** at 72% yield. Three CO peaks at 197.17, 196.88, and 189.20 ppm in the ^{13}C NMR spectrum (Fig. S59†) and three CO stretching peaks at 1901, 1923, and 2020 cm^{-1} in the infrared (IR) spectrum (Fig. S63†) indicate that the Re tricarbonyl complex has an *fac*-Re(bpy)$(CO)_3$Br-type structure.[23] The bulky IS substituent on the imidazolyl group significantly improved the solubility for organic solvents, and **ReDRe** was easily soluble in chloroform, dichloromethane, toluene, and acetonitrile over a 0.1 mM concentration.

Fixation of the dimers *via* covalent bonds in the side chains

To prevent the dissociation of the coordination bond during the catalytic reaction in polar solvents, the dimeric structure was fixed by the ring-closing olefin metathesis reaction on the allyloxy groups at the *meso* positions of the porphyrin.[20,21] First, the metathesis reaction for **ReDRe** was performed using the Grubbs catalyst (1st generation) in dichloromethane (Scheme 2). The reaction progress was monitored with the UV-vis absorption spectrum in pyridine. The split Soret band was observed even in pyridine after the overnight reaction, indicating that all four allyloxy side chains were covalently linked (Fig. S64†). GPC using a pyridine eluent showed a single peak at 21.2 min, suggesting that the reaction proceeded almost perfectly (Fig. S65†). The matrix-assisted laser desorption/ionization-time of flight (MALDI-TOF) mass spectrometry using *trans*-2-[3-(4-*tert*-butylphenyl)-2-methyl-2-propenylidene]-malononitrile (DCTB) as a matrix gave signals corresponding to the covalently linked dimer, *C*-[**Im^{IS}-ZnP-Ph-5Bpy=Re**]$_2$ (**ReD′Re**) in Scheme 2 (Fig. S66†). The ^1H NMR spectrum of the purified **ReD′Re** was compared with that of the nonmetathesized compound **ReDRe** (Fig. S68†). The elimination of the exomethylene signals and a change in the methine signals of the allyl ether groups were observed. The broad signals coupled with the neighboring sp^3-methylene and terminal exomethylene protons were split into two signals at 6.46 and 6.11 ppm, which were assigned to the *E*- and *Z*-olefin isomers, respectively. The molar ratio of the *E*- and *Z*-isomers was 1.9 : 1, suggesting that three isomers exist in a 0.96 : 1:0.27 ratio (Fig. S69†). Therefore, **ReD′Re** is a diastereomixture formed from the two IS groups and the two olefin parts. The diastereomers are difficult to separate in chromatography and are used as a mixture for a catalytic reaction. In addition, three CO peaks for **ReDRe** in the ^{13}C NMR spectrum were split into six peaks for **ReD′Re**, which would result from the *E*- and *Z*-olefin isomers (Fig. S70†).

We confirmed that the ring-closing metathesis reaction of the homodimer **ReDRe** quantitatively proceeds to give the covalently linked dimer, **ReD′Re**. Next, a covalently linked heterodimer in which two types of imidazolyl Zn porphyrins are paired was prepared. Here, to investigate whether a heterodimer can be formed using the porphyrin with the Re complex, a simple *p*-tolyl-substituted Zn porphyrin dimer was used (**D** in Scheme 3). Two types of dimer, **ReDRe** and **D** (1 : 1 molar ratio), were dissolved in pyridine and then the solvent was evaporated. In pyridine, the dimer is dissociated into a pyridine-coordinated monomer. The evaporation of pyridine gives the reorganized dimers. In addition, the ring-closing metathesis reaction was applied to the resulting product in chloroform, giving the heterodimer **ReD′Re**, accompanied by the homodimers **ReD′Re** and **D′**. In the analytical GPC traces of the crude product (Fig. 2), the peaks at 21.2 and 23.8 min were respectively assigned to be **ReD′Re** and **D′** by comparing with the corresponding homodimers. The central peak at 22.1 min was expected as the target **ReD′**. Larger components (oligomers), which were probably formed by the intermolecular metathesis reaction of the

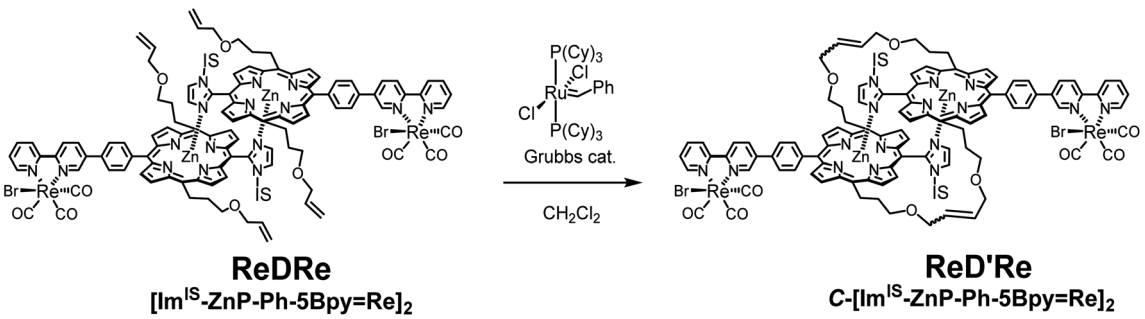

Scheme 2 Ring-closing metathesis reaction of ReDRe.

© 2022 The Author(s). Published by the Royal Society of Chemistry

Open Access Article. Published on 03 augusta 2022. Downloaded on 20.10.2025 1:09:44.
This article is licensed under a Creative Commons Attribution-NonCommercial 3.0 Unported Licence.

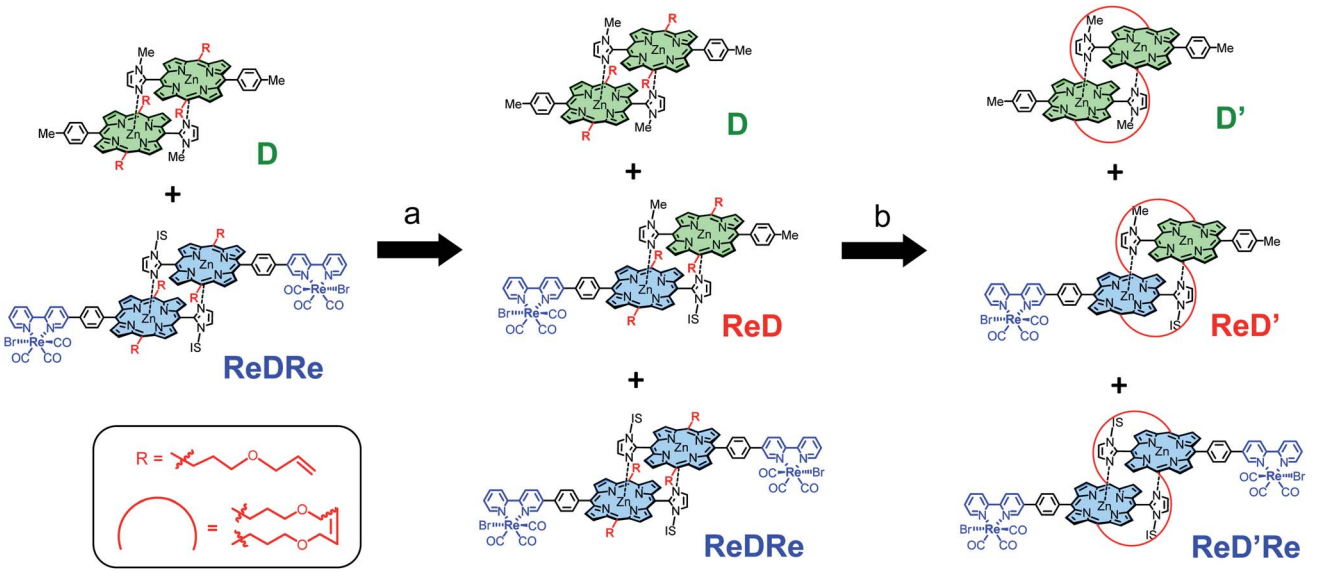

Scheme 3 Synthesis of the heterodimer, **ReD′**. Reagents and conditions: (a) (i) mixing in pyridine at rt, (ii) evaporating the solvent *in vacuo*; (b) Grubbs catalyst (0.5 equiv.), $CHCl_3$, and rt.

dimers, were also observed before 21 min. The MALDI-TOF mass spectrum of each isolated component proved that the species at 22.1 min is **ReD′**. The peak area ratio of **ReD′Re**, **ReD′**, and **D′** in Fig. 2 is a statistical ratio of 0.5 : 1:0.5. When **ReDRe** and **D** were used in a 1 : 4 molar ratio as the starting dimers, the ratio of **ReD′Re**, **ReD′**, and **D′** was 0.04 : 0.26 : 0.70, which was consistent with the ratio (0.04 : 0.32 : 0.64) assumed for the covalently linked dimers to be statistically obtained (Fig. S75†).

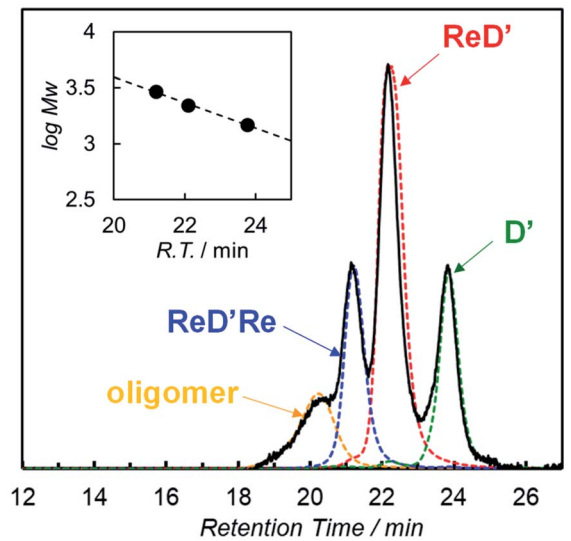

Fig. 2 GPC-high-performance liquid chromatography (HPLC) charts (column: TSK gel $G2500H_{HR} \times 2$ + $G2000H_{HR} \times 1$, eluent: pyridine, flow rate: 1.0 mL min^{-1}, and detection: 440 nm) of the crude product obtained after the metathesis reaction using **ReDRe** and **D** (molar ratio 1 : 1), and the isolated samples by preparative GPC-HPLC. The inset shows the logarithm of molecular weight against the retention time.[9e,24]

Thus, if the proportion of **D**, which can be easily synthesized, is increased, **ReD′** can be efficiently obtained from **ReDRe**. The isolated peaks of **ReD′Re** and **ReD′** have a single Gaussian shape, indicating that the diastereomers originating from the IS and alkene groups hardly affect the molecular size or the hydrodynamic volume.

Photochemical properties

To investigate the substituent effect on the imidazolyl group on the photochemical properties, the UV-vis absorption spectrum of **$[Im^{IS}$-ZnP-Ph-5Bpy$]_2$** was compared with that of **$[Im^{Me}$-ZnP-Ph-5Bpy$]_2$** in chloroform (Fig. S83†). Here, **$[Im^{Me}$-ZnP-Ph-5Bpy=Re$]_2$** is insoluble in chloroform. The two spectra overlap almost completely, suggesting that there is no strong electronic interaction between the IS group and the porphyrin unit and that differences in the photochemical properties due to the presence of isomers of the IS groups would be negligible. Previous studies have reported that the *E*- and *Z*-olefin isomers at the *meso* positions of the porphyrins do not affect the electrochemical and photochemical properties of porphyrins.[20] In fact, the absorption and fluorescence spectra between **ReDRe** and **ReD′Re** in chloroform are almost the same, indicating that the olefin side chains do not affect the electronic state of the porphyrin ring (Fig. S84†).

Fig. 3a shows the UV-vis absorption spectra of **D′**, **ReD′Re**, **ReD′**, and *fac*-Re(bpy)$(CO)_3$Br in DMA, a solvent used for photocatalytic CO_2 reduction.[25] Because DMA weakly coordinates to Zn porphyrin,[18a] the noncovalently linked dimer, **D**, was mostly dissociated into the monomer in the micromolar concentration range. The inset shows a spectral comparison between the Zn porphyrin dimer and *fac*-Re(bpy)$(CO)_3$Br, indicating that the Zn porphyrin unit has a much larger absorption coefficient than the Re(bpy)$(CO)_3$Br unit. The Soret bands split into two peaks (at 414 and 437 nm; $\Delta E = 1270$ cm^{-1} for **ReD′**) due to strong

Open Access Article. Published on 03 augusta 2022. Downloaded on 20.10.2025 1:09:44.
This article is licensed under a Creative Commons Attribution-NonCommercial 3.0 Unported Licence.

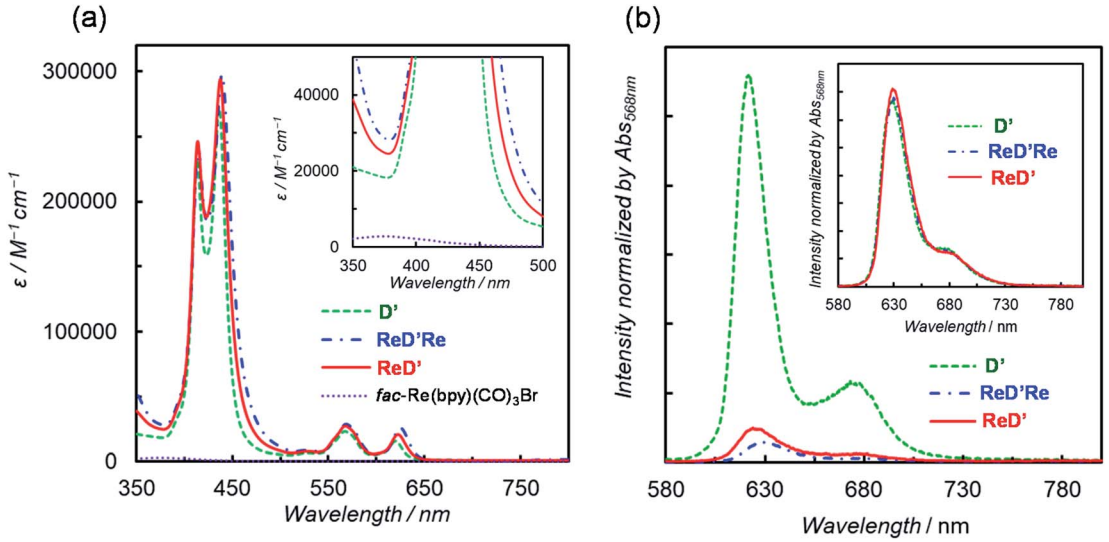

Fig. 3 (a) UV-vis absorption spectra of **D′**, **ReD′**, **ReD′**, and *fac*-Re(bpy)(CO)$_3$Br in DMA. The inset presents the magnification of the near-UV region. (b) Fluorescence spectra of **D′**, **ReD′Re**, and **ReD′** in DMA at 298 K. The inset shows the spectra in toluene. The fluorescence spectra were normalized with the absorbance at the excitation wavelength (λ_{ex} = 568 nm).

exciton coupling between the two porphyrins in the dimer.[19] The excitonic coupling in the Q bands was negligibly small due to the smaller oscillator strengths, and the spectral shape of the Q bands in the dimer was similar to that of the monomeric porphyrin.[9e,19] The introduction of the Re(bpy)(CO)$_3$Br unit caused a slight broadening of the Soret bands and a slight red-shift of the peaks throughout the spectrum (Table 1). The dimer shows a much broader Soret band (caused by the exciton coupling) than that of monomeric Zn porphyrin, enabling the use of a very wide wavelength range of visible light for the photocatalytic reactions.

The fluorescence spectra of **D′**, **ReD′Re**, and **ReD′** are shown in Fig. 3b and their fluorescence quantum yields (Φ_f) in DMA and toluene are summarized in Table 1. The fluorescence intensity decreases in polar DMA (dielectric constant: ε_s = 38.3) as the Re complex is introduced, whereas the fluorescence quenching by the introduction of the Re complex is not observed in nonpolar toluene (ε_s = 2.43) (inset of Fig. 3b). The behavior suggests that the intramolecular electron transfer occurs from the lowest excited singlet state (S_1) of the porphyrin dimer unit to the Re complex unit in **ReD′Re** and **ReD′**.[9a,26] According to the energy levels of the CS state (1.9 eV) estimated from the electrochemical data of **D′** and *fac*-Re(bpy)(CO)$_3$Br and of the S_1 (2.0 eV) of **D′**,[26] the intramolecular electron transfer, the so-called "oxidative quenching",[28] is thermodynamically possible (Fig. S85†). In DMA, the quenching efficiencies of **ReD′** and **ReD′Re** compared to **D′** were 88% and 93%, respectively (Table 1). Assuming that the value of the CS rate constant (k_{CS}) in **ReD′Re** is twice the value in **ReD′**, the ratio of the fluorescence quantum yields of **ReD′Re** to **D** was calculated to be 0.064 (see p. S68 in the ESI†). The value is consistent with the experimental value (0.073), indicating that each Re complex acts independently to quench the S_1 of the porphyrin unit in **ReD′Re**. The quenching efficiencies show that most of the excited energy on the porphyrin mainly produces the CS state between the porphyrin and the Re complex both in **ReD′Re** and **ReD′**. The fluorescence quenching experiments of **D′**, **ReD′**, and **ReD′Re** by BIH gave the Stern–Volmer constants K_{SV} = 3.5 M^{-1}, 0.65 M^{-1}, and 0.32 M^{-1}, respectively (Fig. S86†). The K_{SV} values of **ReD′** and **ReD′Re** were smaller compared with that of **D′** and reflect that the lifetime of the S_1 of the porphyrin is shortened by the formation of the CS state. The lifetimes of **ReD′** and **ReD′Re** were estimated to be 0.37 and 0.18 ns from the Stern–Volmer plots by assuming that the fluorescence quenching process is diffusion-controlled,[18b] which was well consistent with the lifetimes (0.24 and 0.13 ns for **ReD′** and **ReD′Re**, respectively) estimated from the fluorescence quantum yields (see p. S68 in the ESI†).

In a previous report, **ZnP-phen=Re** showed phosphorescence from the Zn porphyrin in Ar-saturated DMA even at rt by strong spin–orbit coupling imposed by the large Re atom in the vicinity.[18b] The phosphorescence was efficiently quenched by an electron donor used in photocatalytic CO_2 reduction, *i.e.*, BIH, indicating that quantitative photoinduced electron transfer

Table 1 Absorption data in DMA and fluorescence data in toluene and DMA[a]

	λ_{abs}/nm (ε/10^4 M^{-1} cm^{-1})	λ_{em}/nm[b]	Φ_f Toluene	Φ_f DMA[c]
D	413 (23), 436 (27) 567 (2.3), 620 (1.6)	622	7.9%	4.2% (1)
ReD′	414 (25), 437 (29) 568 (2.7), 622 (2.0)	625	8.1%	0.50% (0.12)
ReD′Re	414 (24), 439 (30) 568 (2.9), 625 (2.6)	629	8.0%	0.31% (0.073)

[a] Excited at 568 nm. [b] In DMA. [c] The values in parentheses are the ratio to the fluorescence quantum yield of **D**.

© 2022 The Author(s). Published by the Royal Society of Chemistry

Open Access Article. Published on 03 augusta 2022. Downloaded on 20.10.2025 1:09:44.
This article is licensed under a Creative Commons Attribution-NonCommercial 3.0 Unported Licence.

occurred from BIH to the long-lived excited triplet state (T_1) of **ZnP-phen=Re**. In the present systems, no phosphorescence was observed in **ReD′Re** and **ReD′**. It is considered that the distance between the Re atom and the porphyrin unit is too long to induce rt phosphorescence from the Zn porphyrin. In fact, the fluorescence quantum yields of **ReD′Re** and **ReD′** are almost the same as that of **D′** in toluene (Table 1), indicating that the heavy atom effect of the Re atom on porphyrin was negligible. This also supports that the S_1 state of Zn porphyrin was quenched to predominantly produce the CS states in **ReD′Re** and **ReD′**. According to the energy diagram using the phosphorescence spectrum of **D′** at 77 K,[27] the charge-recombination process from the CS states to generate the corresponding T_1 state is thermodynamically possible, as is the generation of ground states (Fig. S85†).

Photocatalytic CO_2 reduction in DMA

Photocatalytic CO_2 reduction was conducted in a DMA solution containing **ReD′** (0.025 mM) and BIH (0.1 M) as the electron donor[18,28] under photoirradiation at 560 nm using light-emitting diode (LED) lamps. A trace amount of CO was produced and its turnover number against the Re atom was only TON_{CO} = 15 after 18 h. By contrast, the addition of either phenol (PhOH, 0.1 M) or TEOA (17 vol%) dramatically increased CO production, and its TON_{CO} reached 780 and 2800 after 18 h, respectively (Fig. 4). PhOH has been reported to act as a proton source to promote the reaction with CO_2 on the Re complex,[29] and TEOA assists trapping CO_2 by forming the Re(bpy)$(CO)_3$(-CO_2-TEOA) species.[30] Herein, CO was selectively produced without forming detectable amounts of H_2, CH_4, and HCOOH. Because TEOA can work as an electron donor,[16c,28] irradiation of a CO_2-saturated DMA-TEOA solution containing **ReD′** was carried out in the absence of BIH as a control experiment. The reaction produced a trace amount of CO (TON_{CO} = 14 after 48 h (Table S1 entry 5†)), indicating that BIH acts as the major electron donor.

The formation of CO using **ReD′**, **ReD′Re**, mixed systems of **D′** and *fac*-Re(bpy)$(CO)_3$Br (1 and 2 equiv. against **D′**), and **ZnP-phen=Re** in CO_2-saturated DMA-TEOA (5 : 1 v/v) solutions containing BIH (0.1 M) is illustrated in Fig. 5. All systems photocatalyzed CO_2 reduction, selectively giving CO. The time profiles of the CO production between **ReD′** and **ReD′Re** were similar, indicating that the absorbed light energy can be used by one Re complex site for the CO_2 reduction reaction and that the catalytic activity of the Re complex is unaffected by another Re complex. From the fluorescence quenching experiment (Fig. S86†), the quenching efficiencies (η_q) of the S_1 states in the presence of [BIH] = 0.1 M can be estimated to be 6% and 3% for **ReD′** and **ReD′Re**, respectively.[28] The quenching efficiency of **ReD′** having one Re complex was higher than that of **ReD′Re** by a factor of 2. If the initial photoinduced electron transfer from BIH occurred mainly through the S_1 state of the porphyrin dimer (reductive quenching),[28] the difference in photocatalytic activities between **ReD′** and **ReD′Re** would be larger. The results indicate that the reductive quenching mechanism can be excluded. Thus, the electron transfer from BIH is expected to occur mainly through the subsequent state after the intramolecular electron transfer (Fig. S85†) (oxidative quenching). The mixed systems of **D′** and *fac*-Re(bpy)$(CO)_3$Br (**Re**) show a mainly relatively lower activity than the connected systems, **ReD′** and **ReD′Re**, but the mixed system using only two equivalents of **Re** shows a moderate activity. In the mixed system, the intermolecular electron transfer from the S_1 state of **D′** to **Re** (oxidative quenching) is unlikely to occur due to the low concentration of **Re**. Considering that the reaction through the

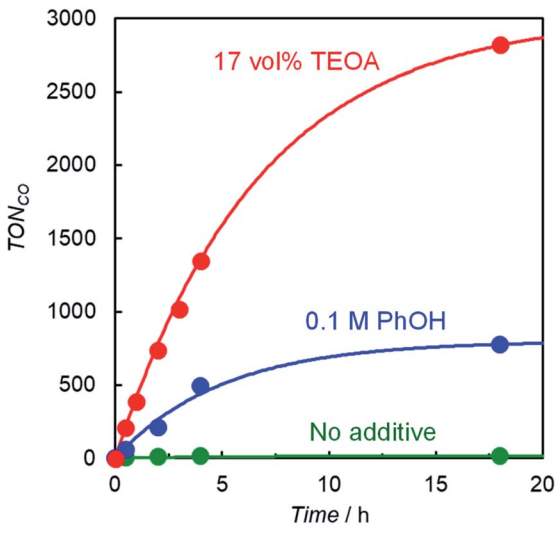

Fig. 4 CO formation with time during irradiation at 560 nm from LED lamps with a merry-go-round apparatus for CO_2-saturated DMA solutions (total 1.0 mL) containing **ReD′** (0.025 mM) and BIH (0.1 M) in the absence (green) and presence of additives ([PhOH] = 0.1 M (blue) and DMA : TEOA = 5 : 1 v/v (red)).

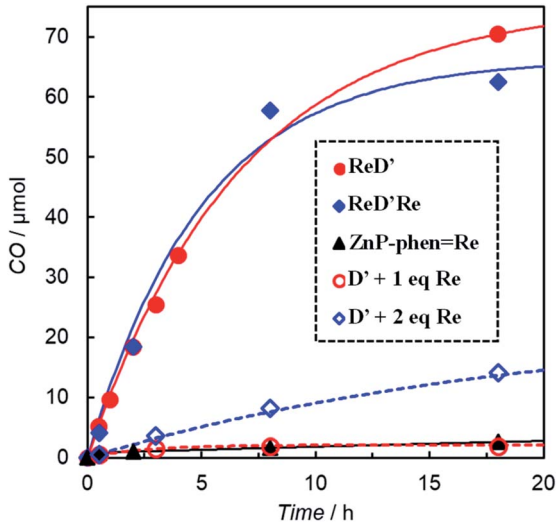

Fig. 5 CO formation with time under irradiation from LED lamps at 560 nm with a merry-go-round apparatus for CO_2-saturated DMA-TEOA (5 : 1 v/v, total 1.0 mL) solutions containing BIH (0.1 M) in the presence of **ReD′** (0.025 mM), **ReD′Re** (0.025 mM), **ZnP-phen=Re** (0.050 mM), and a mixed system of **D′** (0.025 mM) and *fac*-Re(bpy)$(CO)_3$Br (**Re**: 0.025 mM or 0.05 mM).

Open Access Article. Published on 03 augusta 2022. Downloaded on 20.10.2025 1:09:44.
This article is licensed under a Creative Commons Attribution-NonCommercial 3.0 Unported Licence.

T_1 state of **D**′ is thermodynamically difficult (*vide infra*), the reductive quenching from BIH to the S_1 state of **D**′ would start under the condition of high BIH concentration (0.1 M). We believe that the S_1 state of **D**′ has a sufficient lifetime to be quenched by the concentrated BIH (η_q = 26% at 0.1 M from Fig. S86†).

The CO production by **ReD**′ is much larger than that of **ZnP-phen**=**Re** (Fig. 5). The photocatalytic CO_2 reduction upon irradiation at 560 nm of DMA solutions (1.0 mL) containing **ZnP-phen**=**Re** (0.05 mM) and BIH (0.1 M) gave a linear increase in CO production in both the absence and presence of PhOH, whereas the addition of TEOA enhanced the CO production at the initial stage but decreased the durability (Fig. S87†). The TON_{CO} of **ZnP-phen**=**Re** reached 172 after 18 h when PhOH (0.1 M) was added but was 1/16 compared with that of **ReD**′ in DMA-TEOA (Table S1†).

The UV-vis absorption spectral changes of the reaction solutions containing either **ReD**′ or **ZnP-phen**=**Re** during the photocatalytic reactions under CO_2 and Ar atmospheres are shown in Fig. 6. Under the CO_2 atmosphere, the CO formation catalytically proceeded even under micromolar-order concentration conditions of the photocatalysts. The spectrum of **ReD**′ was almost unchanged (Fig. 6a), whereas the original bands of **ZnP-phen**=**Re** significantly decreased, accompanied by the appearance of a band at 620 nm and a featureless broad band at about 700 nm (Fig. 6c), which are assignable to Zn chlorins[16c,d,31] and the one-electron reduced species (OERS) of Zn porphyrin,[32] respectively. Even under an Ar atmosphere, **ReD**′ showed no spectral change (Fig. 6b), suggesting that there is a rapid back-electron transfer process returning to the ground state in **ReD**′. In addition, in **ZnP-phen**=**Re**, TEOA promotes the formation of chlorins and tends to decrease the OERS of porphyrin (Fig. 6c and d). Visible-light irradiation of tetraphenylporphyrin in the presence of aliphatic amine produces chlorins *via* an adduct of porphyrin and amine.[33] Thus, the low catalytic durability of **ZnP-phen**=**Re** in the presence of TEOA (Fig. S87a†) would come

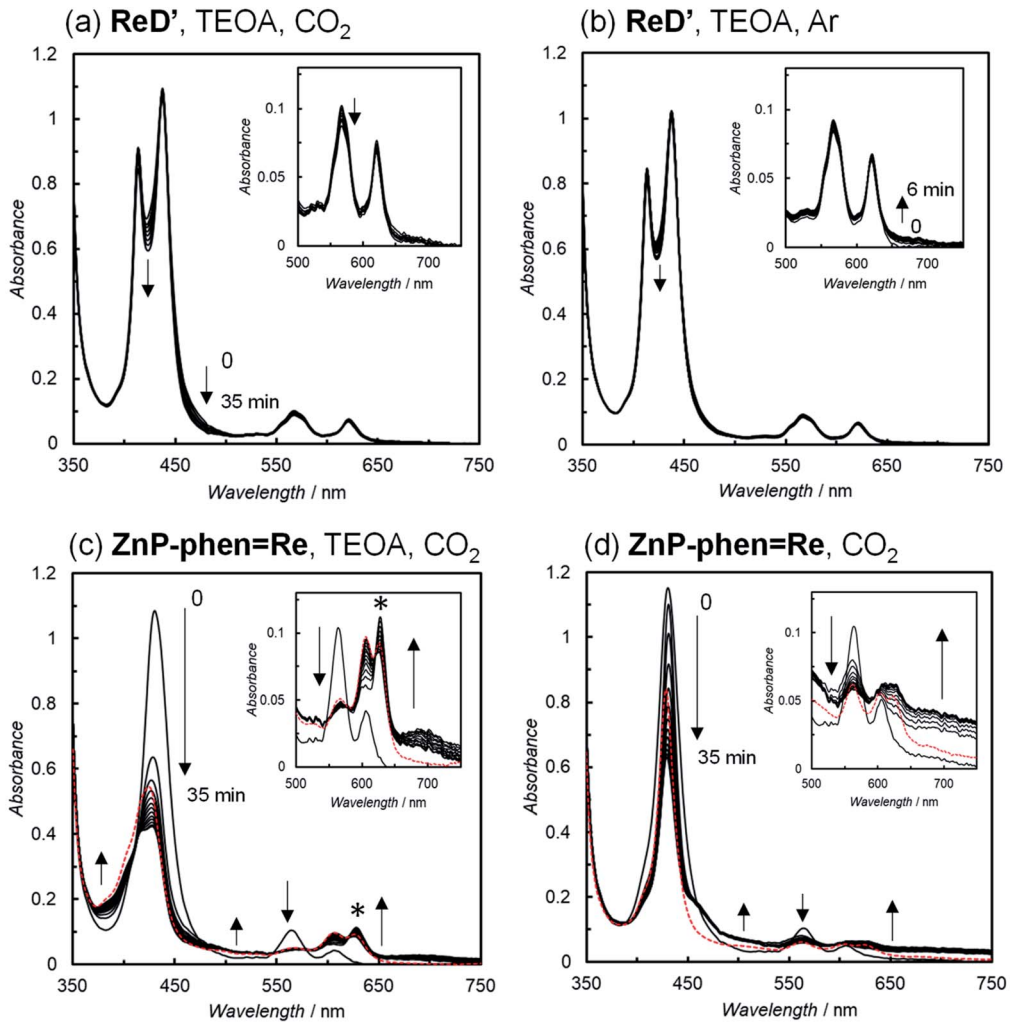

Fig. 6 UV-vis absorption spectral changes of (a, c and d) CO_2– and (b) Ar-saturated DMA solutions in the (a, b and c) presence and (d) absence of 17 vol% TEOA containing the photocatalysts; **ReD**′(a and b; 2.5 μM), **ZnP-phen**=**Re** (c and d; 5.0 μM), and 0.01 M BIH during irradiation at 560 nm (3.5×10^{-8} einstein s^{-1}) from a Xe lamp, 25 °C. The peak marked with an asterisk (*) in Fig. 6c is assigned to chlorins. Red dotted lines show the spectra of resulting solutions after standing for 2 d in the dark.

© 2022 The Author(s). Published by the Royal Society of Chemistry

Open Access Article. Published on 03 augusta 2022. Downloaded on 20.10.2025 1:09:44.
This article is licensed under a Creative Commons Attribution-NonCommercial 3.0 Unported Licence.

Table 2 Quantum yield and products for **ReD′** and **ReD′Re** as a function of excitation wavelength

	Quantum yield (Φ_{CO})[a]			Product/μmol (TON(dimer)[b])		
	420 nm	450 nm	560 nm	CO	H_2	HCOOH
ReD′	0.023	0.032	0.024	70.5 (2820)	n.d.[c]	n.d.[c]
ReD′Re	0.020	0.019	0.016	62.5 (2500)	n.d.[c]	n.d.[c]

[a] Dependence of quantum yield on the excitation wavelength. Quantum yield as a ratio of number of CO and absorbed photons (light intensity: 2.6×10^{-8}, 2.6×10^{-8}, and 3.6×10^{-8} einstein s^{-1} for 420, 450, and 560 nm, respectively (Fig. S89)). A Xe lamp with band path filters was used. [b] A merry-go-round apparatus equipped with LED lamps was used (λ_{ex} = 560 nm). [**ReD′**] = [**ReD′Re**] = 0.025 mM and [BIH] = 0.1 M in CO_2-saturated DMA-TEOA (5 : 1 v/v). The turnover number is based on the porphyrin dimer unit. [c] n.d., not detected.

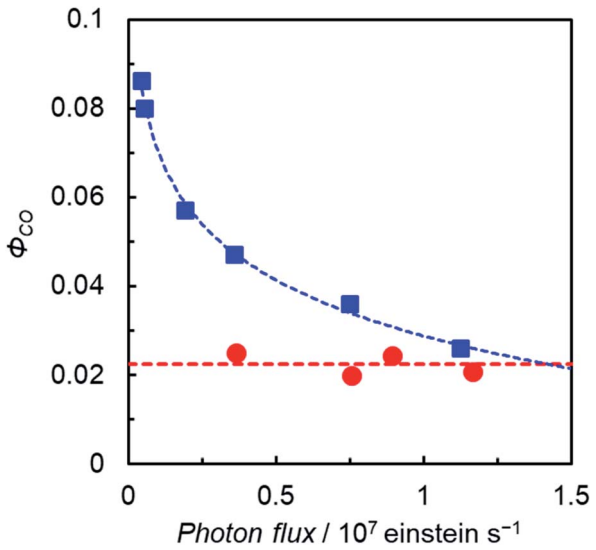

Fig. 7 Φ_{CO} as a function of light irradiation intensity (Xe lamp, λ_{ex} = 560 nm) for **ReD′** (0.1 mM) in DMA-TEOA (5 : 1 v/v) solutions containing BIH (0.1 M) (red circles) and **ZnP-phen=Re** (0.3 mM) in DMA solutions containing BIH (0.05 M) and PhOH (0.1 M) (blue squares).

from chlorin formation. In the absence of TEOA, **ZnP-phen=Re** shows high durability (Fig. S87a†), indicating that the OERS of porphyrin is not a species that directly decomposes the photocatalyst. In contrast to **ZnP-phen=Re**, TEOA is essential for **ReD′** and **ReD′Re** to obtain high catalytic activity and would not react with the porphyrin dimer to form chlorin-producing adducts.

Table 2 summarizes the reaction quantum yields (Φ_{CO}) of CO and the TON_{CO} using **ReD′** and **ReD′Re** in DMA-TEOA (5 : 1 v/v). The Φ_{CO} upon excitations to the upper excited singlet states (S_2) by λ_{ex} = 420 and 450 nm and to S_1 by λ_{ex} = 560 nm has similar values of 2%, indicating that there is no deactivation process from S_2 to S_1. In addition, the Φ_{CO} values are similar between **ReD′Re** and **ReD′**, indicating that one Re complex site is sufficient for the CO_2 reduction reaction and that the electron transfer from BIH to the S_1 of the porphyrin dimer is a minor process in the photocatalytic CO_2 reduction described above. Considering that the Φ_{CO} of **ZnP-phen=Re** is 8% in DMA containing PhOH,[18b] the Φ_{CO} of **ReD′** does not seem to reflect a TON_{CO} of **ReD′** much larger than that of **ZnP-phen=Re** using the merry-go-round apparatus (Fig. 5 and Table S1†). Focusing on the fact that the most different factor between the Φ_{CO} and TON_{CO} measurements is light irradiation intensity,[34] we investigated the dependence of Φ_{CO} on the light intensity and found that the dependence between **ReD′** and **ZnP-phen=Re** was significantly different.

The plots of Φ_{CO} under favorable conditions for **ReD′** and **ZnP-phen=Re** with respect to the light irradiation intensity are shown in Fig. 7. We controlled the light intensity using neutral density filters of 560 nm monochromic light from a Xe lamp with a band path filter. The Φ_{CO} of **ReD′** was independent of the light intensity (red circles in Fig. 7 and S90†), whereas the Φ_{CO} of **ZnP-phen=Re** significantly decreases as the light intensity increases. The decrease in the reaction quantum yield with increasing light intensity is rather commonly observed in photocatalytic systems, because OERS accumulation reduces the catalytic activity due to the inner-filter effect, which is caused by OERS absorption.[35,36] By contrast, the OERS of **ReD′**, which absorbs 560 nm light, did not form during the irradiation (Fig. 6a), resulting in the independence of Φ_{CO} on the light intensity. The strong light from LED lamps with the merry-go-round apparatus lowered the photocatalytic activity of **ZnP-phen=Re** by the inner-filter effect of the OERS, whereas the photocatalytic activity of **ReD′** was not lowered due to no OERS accumulation (Fig. 6a). The independence of **ReD′** on light intensity was also observed on the TON_{CO} using the merry-go-round apparatus (Fig S91†).

Another interesting difference between **ReD′** and **ZnP-phen=Re** is the dependence of the catalytic activity on the BIH concentration. The catalytic activity of **ZnP-phen=Re** does not depend on the concentration of BIH because the photoinduced electron transfer from BIH occurs *via* the long-lived T_1 (K_{SV} = 180 000 M^{-1}) with reductive quenching from the T_1 state.[18b] Upon excitation at 560 nm, the overlaid plots of CO production against the absorbed photon using 0.01 M and 0.05 M BIH show the independence of the BIH concentration in **ZnP-phen=Re** (Fig. S92†). By contrast, the Φ_{CO} and TON_{CO} strongly depend on the BIH concentration in **ReD′** (Fig. 8 and S93†). The simulation of the quenching efficiencies on the state that mediates the electron transfer from BIH gave the same order values of K_{SV} = 8 M^{-1} and 15 M^{-1} from the plots of Φ_{CO} and TON_{CO}, respectively. The obtained value was much smaller than that of **ZnP-phen=Re**, suggesting that a relatively short-lived state such as the CS state ($ZnP^{\bullet+}$–$Re^{\bullet-}$ in Fig. S85†) contributes to the electron transfer from BIH. In fact, the coordination of the imidazolyl group to the Zn porphyrin lowers the energy level of T_1 (ref. 27) and shifts the reduction potential of the porphyrin to the negative side,[26,37] so that the electron transfer from BIH to the T_1 of the porphyrin dimer forming the OERS of the porphyrin is thermodynamically unfavorable (Fig. S94†).

Photocatalytic CO_2 reduction in DMSO

The above results indicate that **ReD′** (**ReD′Re**), which has the porphyrin dimer as the photosensitizer, proceeds by a different

Open Access Article. Published on 03 augusta 2022. Downloaded on 20.10.2025 1:09:44.
This article is licensed under a Creative Commons Attribution-NonCommercial 3.0 Unported Licence.

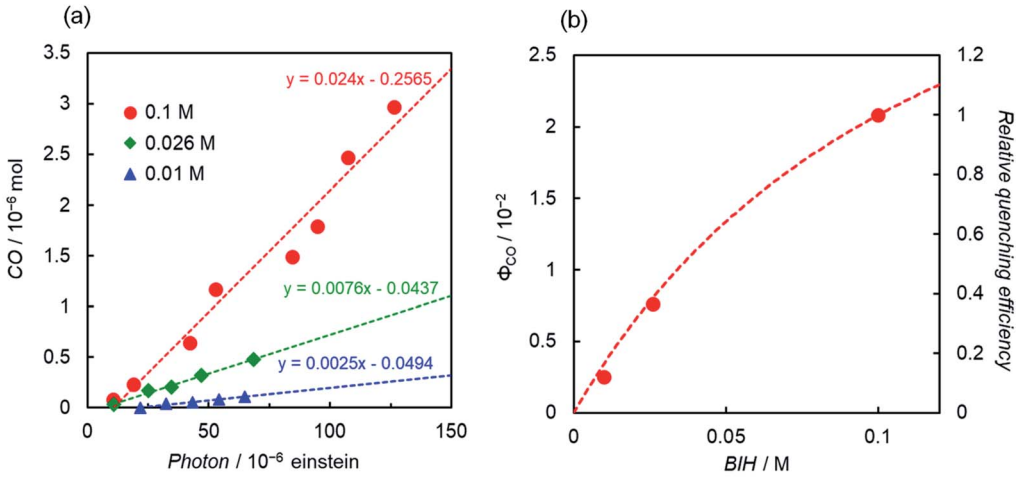

Fig. 8 (a) CO formation during irradiation at 560 nm (Xe lamp, 3.6×10^{-8} einstein s^{-1}) using BIH (red circle, 0.1 M; green diamond. 0.026 M; blue triangle, 0.01 M) and **ReD′** (0.1 mM) in CO_2-saturated DMA-TEOA (5 : 1 v/v). (b) The reaction quantum yield as a function of BIH concentration. The quenching efficiency relative to η_q at [BIH] = 0.1 M was calculated using η_q = [BIH] K_{SV}/(1 + [BIH] K_{SV}) assuming K_{SV} = 8 M^{-1}.

mechanism from that of **ZnP-phen=Re**, and shows an extremely high activity under irradiation with strong light. However, the bond distance and direction between the porphyrin and the Re complex in **ReD′** (**ReD′Re**) were different from those of **ZnP-phen=Re**. The differences could affect the catalytic activity. Therefore, to clarify whether the dimeric structure of the porphyrin contributes to the high activity, photocatalytic reactions were performed under the same conditions using **ReDRe** and **ReD′Re** (Scheme 2) in a coordination solvent of DMSO. Here, DMSO is a suitable solvent for photocatalytic CO_2 reduction using a Re diimine tricarbonyl complex in the presence of BIH and TEOA.[38] Under micromolar-order concentration conditions, **ReDRe** dissociated into the corresponding monomer (Fig. 9). The first oxidation and reduction potentials of the porphyrin dimer **D′** and monomer **D** (Scheme 3) were almost the same in DMSO in differential pulse voltammetry (DPV) (Fig. S95†) and the potentials of **ReD′Re** were similar to those in DMA. In addition, the fluorescence of the monomer prepared from **ReDRe** in DMSO was quenched by the Re complex unit, indicating that the intramolecular electron transfer from the S_1 of the porphyrin unit to the Re complex unit would occur in the monomer as well as in the dimer (Fig. S96†).

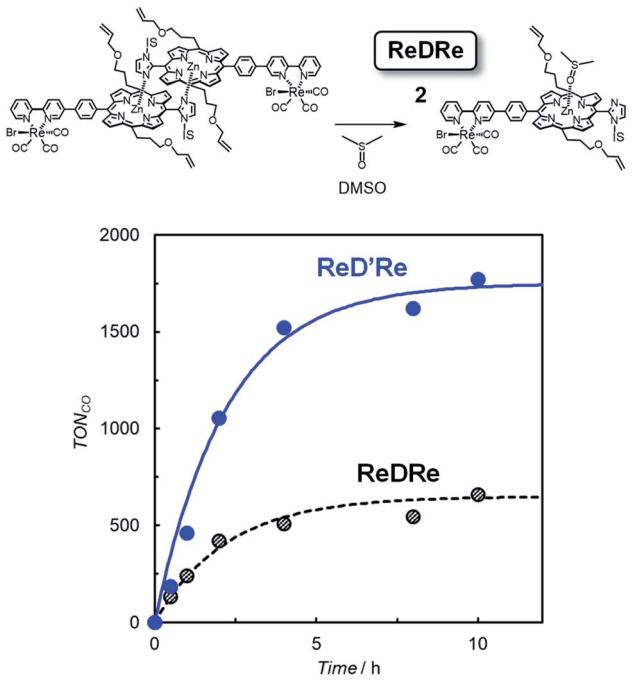

Fig. 9 (Top) dissociation of the porphyrin dimer (**ReDRe**) into porphyrin monomers in DMSO. (Bottom) CO formation with time during irradiation at 560 nm from LED lamps with a merry-go-round apparatus for CO_2-saturated DMSO-TEOA (5 : 1 v/v) solutions containing **ReD′Re** (2.5 μM) and **ReDRe** (2.5 μM) in the presence of BIH (0.01 M). The TON_{CO} is calculated against the Re atom.

The CO production with time using dilute **ReDRe** and **ReD′Re** of the micromolar range (2.5 μM) is shown in Fig. 9. From the UV-vis absorption spectrum (Fig. 10a inset), **ReDRe** completely dissociates into the monomeric structure under these reaction conditions (2.5 μM **ReDRe**). The Q band is inert to whether the porphyrin is the monomer or dimer, and the initial absorbance of **ReDRe** and **ReD′Re** at 560 nm is almost the same even in DMSO. Thus, 560 nm was selected as the excitation wavelength of the photocatalytic reaction. In the system using the porphyrin dimer (**ReD′Re**), the TON_{CO} was much larger than in the system using the porphyrin monomer (**ReDRe**). The UV-vis spectral changes during irradiation show that the spectrum of **ReD′Re** hardly changed (Fig. 10), but the monomer spectrum shows significant reductions in both the Soret and Q bands (Fig. 10a inset), indicating that the porphyrin monomer decomposed into colorless species. To investigate the degradation process, we carried out the irradiation of a CO_2-saturated DMSO-TEOA (5 : 1 v/v) containing a higher concentration of **ReDRe** (10 μM) in the presence of BIH (0.05 M). The UV-vis absorption spectrum after the irradiation for 7 h (Fig. S97†), when the rate of CO formation became slow, showed

© 2022 The Author(s). Published by the Royal Society of Chemistry

Open Access Article. Published on 03 augusta 2022. Downloaded on 20.10.2025 1:09:44.
This article is licensed under a Creative Commons Attribution-NonCommercial 3.0 Unported Licence.

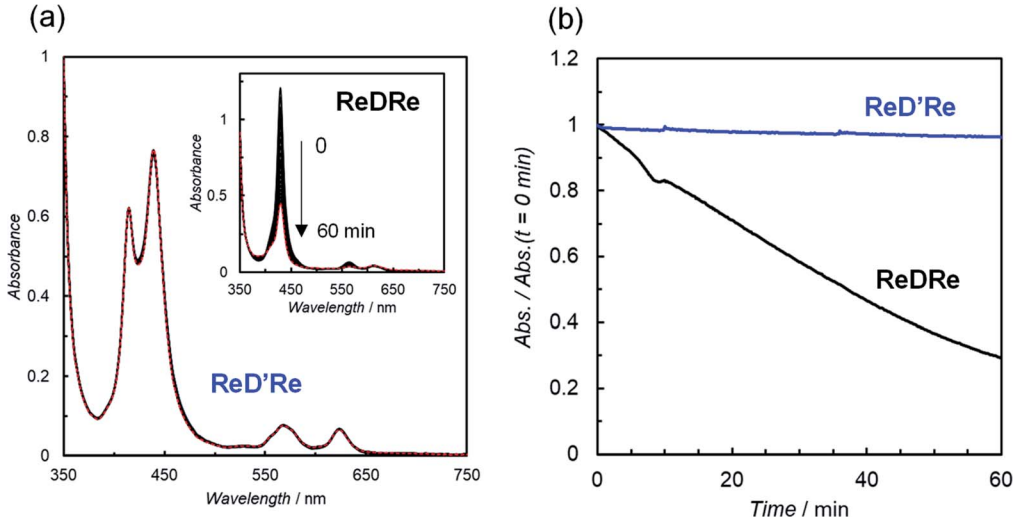

Fig. 10 (a) UV-vis absorption spectral change of a CO_2-saturated DMSO-TEOA (5 : 1 v/v) solution containing BIH (0.01 M) and **ReD′Re** (2.5 μM) during irradiation at 560 nm (Xe lamp, 3.5×10^{-8} einstein s^{-1}) and 25 °C. Inset shows change using **ReDRe** instead of **ReD′Re**. Red dotted lines show the spectra after the irradiation for 60 min. (b) Relative absorbance with time at 430 nm of the reaction solutions during the irradiation.

the appearance of distinct absorption peaks at 500 and 760 nm for bacteriochlorins[39] and 610 nm for chlorins.[16c,40] Thus, as shown in the literature,[16c] it is though that the monomeric porphyrin is degraded to colorless species *via* chlorins and bacteriochlorins, whose process is initiated by two electron reduction of Zn porphyrin (Fig. S98a†). The system using **ReD′Re** reaches $TON_{CO} \sim 1800$ (based on the Re atom). Considering that the equivalent of added BIH against the Re atom was 2000, BIH donated two electrons and an almost quantitative amount of added BIH was consumed.[28,41]

Reaction mechanisms in systems using the porphyrin dimer

Based on the above results, a plausible reaction mechanism is shown in Fig. 11. The porphyrin dimer in **ReD′** and **ReD′Re** can absorb a wide wavelength range of visible light to give the S_1 state, which would efficiently produce the CS state by intramolecular electron transfer. Although the CS state can be stabilized by the dimeric structure in **ReD′** and **ReD′Re**,[7] a rapid back-electron transfer process generally competes with the catalytic reaction. The nonspectral change in **ReD′** under an Ar atmosphere (Fig. 6b) is explained by the rapid back-electron transfer process. The proton promotes the formation of an adduct between the reduced Re complex and CO_2,[42] and TEOA coordinates to the Re complex in the ground state to form an adduct with CO_2.[30,38] Thus, with the assistance of PhOH or TEOA, the transient reduced Re complex would rapidly react with CO_2 to afford a more stable reaction intermediate that suppresses the back-electron transfer. Considering the fact that the formation of Re–COOH should be rather slower as reported in the literature,[43] in the presence of PhOH the hole scavenging process by BIH more probably occurs before the Re–C bond formation. In this mechanism, BIH is used to neutralize the cation radical of the porphyrin to give the ground state porphyrin, and no long-lived OERS of the porphyrin was formed.

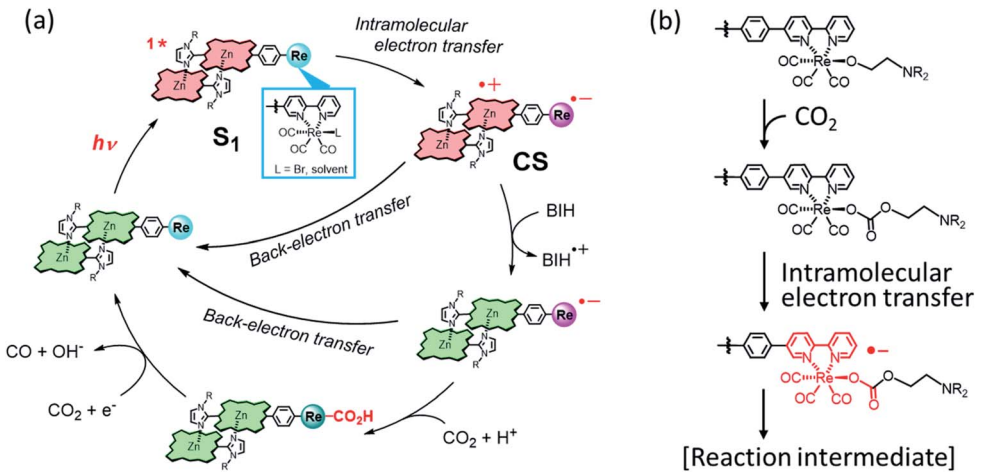

Fig. 11 (a) A plausible reaction mechanism of **ReD′** (**ReD′Re**) in the presence of a proton source such as PhOH.[42,43] (b) The CO_2-capturing reaction with the Re(I) complex with the assistance of TEOA.[30,38]

Open Access Article. Published on 03 augusta 2022. Downloaded on 20.10.2025 1:09:44.
This article is licensed under a Creative Commons Attribution-NonCommercial 3.0 Unported Licence.

In **ZnP-phen**=**Re**, it is thought that the adjacent Re atom enhances the intersystem crossing from the S_1 to the T_1 of porphyrin and the initial electron transfer mainly occurs *via* the long-lived T_1.[18b] Thus, the efficient electron transfer from BIH to T_1 allows the catalytic reaction to proceed with the same activity even at a low concentration of the electron donor. However, although the accumulation of the porphyrin's OERS would not directly lead to a decrease in the catalytic durability, the inner-filter effect by the OERS under strong light irradiation lowers the reaction efficiency. By contrast, the formation of the CS state in **ReD′** and **ReD′Re** causes independence of the CO_2 reduction reaction rate on light intensity because no species that inhibits light absorption is accumulated.

The porphyrin dimer delocalizes the radical cation over the two porphyrin units, giving the stable CS state that can promote the subsequent reaction before the back-electron transfer. The dimeric structure has been reported to accelerate the CS rate and decelerate the charge-recombination rate.[7] **ReD′** had a higher quenching efficiency in DMA against **D′** (88% in Fig. 3b and Table 1) than **ReDRe** against **D** in DMSO (73% in Fig. S96†), which might support the acceleration of the CS rate. The dimer is superior to the monomer in durability (Fig. 9). Judging from the UV-vis spectrum (Fig. S97†), the irradiation of the DMSO-TEOA solution containing **ReDRe** (monomer) in the presence of BIH gave chlorins and bacteriochlorins. Because BIH produces a very strong reductant $BI^{\bullet}$,[28,41] the two-electron reduced species on the porphyrin unit can be generated. Thus, it is thought that the monomeric structure is easily decomposed by two electron reduction, whereas the dimeric structure can suppress degradation by sharing electrons between the two porphyrins of the dimer (Fig. S98b†), even when a two-electron reduced species is produced on the porphyrin unit.[44] In the case of **ZnP-phen**=**Re**, the high durability might be due to the proximity between Re and the porphyrin, causing rapid electron transfer to the Re complex unit and preventing the accumulation of two electrons on the porphyrin. The detailed reaction mechanisms of **ReD′** and **ReD′Re** in addition to **ZnP-phen**=**Re** are currently under investigation using time-resolved measurements.

Conclusion

The special-pair mimic porphyrin dimer was used here as a photosensitizer in a photocatalytic reaction for the first time. Using the fact that the coordination bond of the dimer can be easily rearranged and that the coordination structure can be fixed by a covalent bond by the ring-closing metathesis reaction, dimers having Re complex(es) on either one side (**ReD′**) or two sides (**ReD′Re**) have been synthesized. The photocatalytic CO_2 reductions using **ReD′** and **ReD′Re** selectively gave CO, the reaction quantum yield of which was estimated to be 2%, independent of the excitation wavelength, light intensity, and number of Re complex units. A high TON_{CO} reaching >2800 after 18 h was observed in **ReD′** under irradiation of relatively strong light, which is an order of magnitude higher than the value (172 after 18 h) of **ZnP-phen**=**Re** under the optimal conditions. The high catalytic activity stems from the fact that the absorption spectrum of the dimer remains almost unchanged during the irradiation and there is no deactivation caused by the internal filter effect that the OERS absorbs light as observed in general photosensitizers. It is thought that the catalytic reaction proceeds *via* the CS state formed by the intramolecular electron transfer from the S_1 of the porphyrin unit to the Re complex unit, and that BIH neutralizes the cation radical of the porphyrin. Thus, the excessive OERS does not form during the irradiation. In addition, it was shown that the dimeric structure contributes to the improvement of the catalytic durability of CO_2 reduction by sharing electrons between the two porphyrins of the dimer. In this work, we prepared a heterodimer of **ReD′** using a simple porphyrin **D** having a tolyl group. The simple porphyrin can be substituted with an imidazolyl Zn porphyrin having more functional units. As a result, it may be possible to create functional heterodimers that can bind to semiconductors and supramolecular systems such as chain structures and cyclic structures with a higher absorption ability.

Experimental section

General procedure

All chemicals and solvents were of commercial reagent quality and were used without further purification unless otherwise stated. Dry diethyl ether was prepared by distillation over benzophenone/Na. DMA was dried over molecular sieves of size 4 Å and distilled under reduced pressure. The Grubbs catalyst (1st generation), benzylidene-bis(tricyclohexylphosphine) dichlororuthenium, was purchased from Aldrich. 1-Methylimidazole-2-carbaldehyde, *meso*-(3-allyloxypropyl)dipyrromethane, and BIH were synthesized according to the literature.[9,45] FINEOXOCOL180 was provided by Nissan Chemical Corporation. Super dehydrated *N*,*N*-dimethylformamide (DMF) and tetrahydrofuran (THF) were purchased from Fujifilm Wako Pure Chemical Corporation. TEOA was distilled under reduced pressure. The reaction was monitored on silica-gel $60F_{254}$ TLC plates (Merck). Silica-gels utilized for column chromatography were purchased from Kanto Chemical Co. Inc.: Silica-Gel 60N (Spherical, Neutral) 63–210 μm and 40–50 μm (Flash). ^{1}H and ^{13}C NMR, distortionless enhancement by polarization transfer 135 (DEPT 135), ^{1}H–^{1}H correlation spectroscopy (COSY), ^{1}H–^{13}C heteronuclear single quantum correlation (HSQC), and ^{1}H–^{13}C heteronuclear multiple bond correlation (HMBC) spectra were recorded by using a JEOL JNMECS-300, JNMECZ-400, and JNMECS-500. Chemical shifts were recorded in parts per million (ppm) relative to tetramethylsilane. UV-vis absorption spectra were collected using square cells (path length = 1.0 cm) on JASCO V-650 and V-660 spectrometers, and a Asahi Spectra PRA-201. Steady-state emission spectra were collected on a Hitachi F-4500 spectrometer and corrected for the response of the detector system. The fluorescence intensities were normalized at the absorption of the excitation wavelength. Fluorescence quantum yields were determined from the integrated ratios of the fluorescence spectra relative to that of ZnTPP ($\Phi_f = 3.3\%$ in toluene).[46] Their values were corrected with the refractive indices of the used solvents. Hi-resolution MALDI–TOF mass

© 2022 The Author(s). Published by the Royal Society of Chemistry

Open Access Article. Published on 03 augusta 2022. Downloaded on 20.10.2025 1:09:44.
This article is licensed under a Creative Commons Attribution-NonCommercial 3.0 Unported Licence.

spectra were collected on a JEOL JMS S-3000 with dithranol or *trans*-2-[3-(4-*tert*-butylphenyl)-2-methyl-2-propenylidene]-malononitrile (DCTB) as a matrix. FTIR spectra were recorded in KBr using a JASCO FT/IR-4600. Analytical GPC-HPLCs using pyridine as the eluent were performed on a PU-2080plus and MD-2018plus (JASCO) system equipped with two TSK G2500H_{HR} (Tosoh, exclusion limit: 20 000 Da) and one TSK G2000H_{HR} (Tosoh, exclusion limit: 10 000 Da) columns. Preparative HPLCs were carried out on an LC-908 (JAI) attached to one TSK G2500H_{HR} and one G2000H_{HR} columns eluted with pyridine. The differential pulse voltammogram (DPV) was recorded using an ALS-H/CHI Model 612E electrochemical analyzer in a micro-cell equipped with a glassy carbon working electrode (ϕ 1.6 mm) and a Pt counter electrode. The micro-cell was connected *via* a Luggin capillary with a reference electrode of Ag/$AgNO_3$ (10 mM in DMSO). Tetrabutylammonium hexafluorophosphate (^{n}Bu$_4$NPF_6) recrystallized from ethyl acetate was used as a supporting electrolyte. Ferrocene was used as an external standard, and all potentials were referenced to the ferrocene/ferrocenium couple ($E_{1/2}$ = +0.191 V *vs.* Ag/$AgNO_3$).

5-(4-Iodophenyl)-15-(1-isostearylimidazole-2-yl)-10,20-bis(3-allyloxypropyl)porphyrin (Im^{IS}-H_2P-PhI). In a three-necked 500 mL flask, **Im^{IS}-CHO** (420 mg, 1.2 mmol), 4-iodobenzaldehyde (270 mg, 1.2 mmol), and *meso*-(3-allyloxypropyl)dipyrromethane (740 mg, 3.0 mmol), and $CHCl_3$ (300 mL) were placed. The mixture was degassed by bubbling with Ar gas for 15 min and then trifluoroacetic acid (TFA, 0.39 mL, 4.8 mmol) in $CHCl_3$ (*ca.* 2 mL) was slowly added. After being stirred for 3.5 h at rt, the mixture was added by triethylamine (0.68 mL, 4.9 mmol) and *p*-chloranil (1.4 g, 5.2 mmol) and stirred at rt overnight. The resulting mixture was evaporated to dryness and the residue was purified with an alumina column (eluent: $CHCl_3$/acetone = 10/1) and silica gel columns (eluent: $CHCl_3$ → $CHCl_3$/acetone = 10/1). The collected solution was evaporated to dryness, giving a purple solid (230 mg, 19% yield). TLC (silica gel, $CHCl_3$/acetone = 10/1) R_f = 0.5; MALDI-TOF-mass (dithranol) *m*/*z* [M + H]$^+$ 1027.5002, calcd for [$C_{59}H_{76}IN_6O_2$]$^+$ 1027.5068; ^{1}H NMR (400 MHz, $CDCl_3$) δ/ppm = 9.54 (m, 2H, β-pyrrole), 9.49 (m, 2H, β-pyrrole), 8.96–8.76 (m, 4H, β-pyrrole), 8.12 (d, J = 8.7 Hz, 1H, phenylene), 8.12 (d, J = 8.7 Hz, 1H, phenylene), 7.98 (m, 1H, phenylene), 7.86 (m, 1H, phenylene), 7.74 (s, 0.4H, Im), 7.72 (s, 0.6H, Im), 7.52 (s, 0.4H, Im), 7.50 (s, 0.6H, Im), 6.09 (m, 2H, –CH=), 5.44 (d, J = 17 Hz, 2H, =CH_2), 5.28 (d, J = 10 Hz, 2H, =CH_2), 5.10 (m, 4H, –$CH_2CH_2CH_2$–), 4.08 (d, J = 5.5 Hz, 4H, –OCH_2–), 3.85–8.40 (m, 2H, CH_2), 3.66 (m, 4H, –$CH_2CH_2CH_2$–), 2.78 (m, 4H, –$CH_2CH_2CH_2$–), 1.38–8.40 (m, 2H, CH_2), 1.38–(–0.80) (m, 35H), −2.64 (s, 0.6H, NH), −2.66 (s, 0.4H, NH);^{13}C NMR (100 MHz, $CDCl_3$) δ/ppm = 150–145 (C), 148.95 (C), 148.66 (C), 142.30 (C), 142.27 (C), 136.10 (CH), 135.85 (CH), 135.17 (CH), 131.99–131.50 (CH), 131.22–130.74 (CH), 129.66–128.90 (CH), 128.57 (CH), 128.51 (CH), 128.12 (CH), 128.10 (CH), 128.02–127.55 (CH), 121.41 (CH), 121.29 (CH), 120.33 (CH), 120.27 (CH), 119.61 (C), 119.56 (C), 119.48 (C), 119.09 (C), 119.02 (C), 117.00 (CH_2), 105.31 (C), 105.26 (C), 105.11 (C), 94.21 (C), 72.14 (CH_2), 69.29 (CH_2), 51.20 (CH_2), 50.75 (CH_2), 50.68 (CH_2), 50.46 (CH_2), 49.39 (CH_2), 49.29 (CH_2), 49.20 (CH_2), 49.12 (CH_2), 48.93 (CH_2), 47.70 (CH or CH_3), 47.42 (CH_2), 47.21 (CH_2), 46.72 (CH_2), 46.32 (CH_2), 37.96 (CH_2), 37.47 (CH_2), 37.23 (CH_2), 36.90 (CH_2), 36.59 (CH_2), 31.44 (CH_2), 31.18 (C), 30.93 (C), 30.75 (C), 30.61 (C), 30.55 (C), 30.23 (C), 30.03 (CH or CH_3), 29.89 (CH or CH_3), 29.86 (CH or CH_3), 29.64 (CH or CH_3), 29.41 (CH or CH_3), 29.18 (CH or CH_3), 29.10 (CH or CH_3), 29.03 (CH or CH_3), 28.61 (CH or CH_3), 28.38 (CH or CH_3), 28.16 (CH or CH_3), 28.00 (CH or CH_3), 27.77 (CH or CH_3), 26.85 (CH_2), 26.72 (CH_2), 24.61 (CH_2), 24.55 (CH_2), 22.51 (CH or CH_3), 22.15 (CH or CH_3), 22.08 (CH or CH_3), 22.01 (CH or CH_3), 16.61 (CH or CH_3), 16.51 (CH or CH_3), 16.40 (CH or CH_3), 16.22 (CH or CH_3).

Zinc(II) 5-(4-iodophenyl)-15-(1-isostearylimidazole-2-yl)-10,20-bis(3-allyloxypropyl)porphyrin ([Im^{IS}-ZnP-PhI]$_2$). Zinc(II) acetate (330 mg, 1.8 mmol) in methanol (*ca.* 3 mL) was added to a solution of **Im^{IS}-H_2P-PhI** (230 mg, 0.22 mmol) in $CHCl_3$ (230 mL). The mixture was stirred overnight at rt. The resulting solution was washed with water. The organic layer was dried over anhydrous Na_2SO_4 and evaporated to dryness, affording the titular compound as a purple solid (230 mg, 96% yield). TLC (silica gel, $CHCl_3$/acetone = 10/1) R_f = 0.9; MALDI-TOF-mass (dithranol) *m*/*z* [M + H]$^+$ 1089.4229, calcd for [$C_{59}H_{74}IN_6O_2Zn$]$^+$ 1089.4204; ^{1}H NMR (400 MHz, $CDCl_3$) δ/ppm = 9.63 (m, 2H, β-pyrrole), 9.00 (m, 2H, β-pyrrole), 8.91 (m, 2H, β-pyrrole), 8.43 (m, 1H, phenylene), 8.27 (d, J = 7.9 Hz, 1H, phenylene), 8.11 (d, J = 7.9 Hz, 1H, phenylene), 7.89 (m, 1H, phenylene), 6.22 (m, 2H, –CH=), 5.57 (m, 2H, =CH_2), 5.56 (s, 1H, Im), 5.42 (m, 2H, β-pyrrole), 5.36 (d, J = 10 Hz, 2H, =CH_2), 5.22 (m, 4H, –CH_2-CH_2CH_2–), 4.24 (m, 4H, –OCH_2–), 3.92 (m, 4H, –$CH_2CH_2CH_2$–), 3.02 (m, 4H, –$CH_2CH_2CH_2$–), 2.06 (m, 1H, Im), 1.84–1.55 (m, 2H, CH_2), 0.30–(–1.77) (m, 35H); ^{13}C NMR (100 MHz, $CDCl_3$) δ/ppm = 151.14 (C), 150.05 (C), 148.65 (C), 148.38 (C), 146.02 (C), 144.10 (C), 136.47 (CH), 136.41 (CH), 135.59 (CH), 135.53 (CH), 135.46 (CH), 135.32 (CH), 131.63 (CH), 131.50 (CH), 129.45 (CH), 129.31 (CH), 128.48 (CH), 127.84 (CH), 121.20 (CH), 119.60 (C), 119.33 (C), 117.66 (CH), 116.88 (CH_2), 96.93 (C), 93.41 (C), 72.18 (CH_2), 70.20 (CH_2), 50.53 (CH_2), 50.22 (CH_2), 50.01 (CH_2), 49.91 (CH_2), 47.75 (CH_2), 47.58 (CH_2), 47.38 (CH_2), 47.31 (CH_2), 46.50 (CH_2), 45.81 (CH or CH_3), 45.40 (CH or CH_3), 45.21 (CH or CH_3), 44.98 (CH or CH_3), 44.800 (CH or CH_3), 38.74 (CH_2), 35.60 (CH_2), 35.44 (CH_2), 32.16 (CH_2), 30.26 (C), 30.21 (C), 30.16 (C), 30.05 (C), 29.80 (CH_2), 29.60 (CH or CH_3), 29.44 (CH or CH_3), 29.39 (CH or CH_3), 29.31 (CH or CH_3), 28.65 (CH or CH_3), 28.48 (CH or CH_3), 29.21 (CH or CH_3), 27.01 (CH or CH_3), 26.86 (CH or CH_3), 26.63 (CH or CH_3), 21.92 (CH or CH_3), 21.56 (CH or CH_3), 21.27 (CH or CH_3), 15.74 (CH or CH_3).

Zinc(II) 5-{4-(2,2′-bipyrid-5-yl)phenyl}-15-(1-isostearylimidazole-2-yl)-10,20-bis(3-allyloxypropyl)porphyrin ([Im^{IS}-ZnP-Ph-5Bpy]$_2$). In a 100 mL three-necked flask, **[Im^{IS}-ZnP-PhI]$_2$** (310 mg, 0.28 mmol), 5-(4,4,5,5-tetramethyl-1,3,2-dioxaborolan-2-yl)-2,2′-bipyridine (120 mg, 0.42 mmol), Cs_2CO_3 (26.0 mg, 0.80 mmol), toluene (30 mL), DMF (15 mL), and water (2.3 mL) were placed. The mixture was degassed by freeze–thaw cycles and replaced with Ar gas and Pd(PPh_3)$_4$ (68 mg, 0.059 mmol) was added and stirred at 90 °C for 4 h. $CHCl_3$ (100 mL) and water (100 mL) were added to the resulting solution, and the organic layer was washed with water (100 mL) and brine (100 mL). The organic layer was passed through Phase Separator paper (Whatman). The solvent was evaporated to dryness and

Open Access Article. Published on 03 augusta 2022. Downloaded on 20.10.2025 1:09:44.
This article is licensed under a Creative Commons Attribution-NonCommercial 3.0 Unported Licence.

the residue was purified with a flush silica gel column (eluent: $CHCl_3$ → $CHCl_3$/acetone = 10/1). Further purification by precipitation with $CHCl_3$, methanol and water afforded 280 mg (89% yield) of the titular compound as a dark purple solid. TLC (silica gel, $CHCl_3$/acetone = 10/1) R_f = 0.1; MALDI-TOF-mass (dithranol) *m*/*z* $[M + H]^+$ 1117.5768, calcd for $[C_{69}H_{81}N_8O_2Zn]^+$ 1117.5768; ^{1}H NMR (500 MHz, $CDCl_3$) δ/ppm = 9.67 (m, 2H, β-pyrrole), 9.40 (s, 1H, bpy 6), 9.11 (m, 2H, β-pyrrole), 8.92 (m, 2H, β-pyrrole), 8.82 (m, 2H, phenylene and bpy 6′), 8.71 (d, *J* = 7.9 Hz, 1H, bpy 3), 8.61 (d, *J* = 7.7 Hz, 1H, bpy 3′), 8.49 (d, *J* = 7.9 Hz, 1H, bpy 4), 8.31 (brs, 1H, phenylene), 8.26 (d, *J* = 7.6 Hz, 1H, phenylene), 8.10 (brs, 1H, phenylene), 7.94 (t, *J* = 7.7 Hz, 1H, bpy 4′), 7.41 (t, *J* = 7.7 Hz, 1H, bpy 5′), 6.21 (m, 2H, -CH═), 5.56 (s, 1H, Im), 5.54 (m, 2H, ═CH_2), 5.44 (m, 2H, β-pyrrole), 5.37 (m, 2H, ═CH_2), 5.26 (m, 4H, –$CH_2CH_2CH_2$–), 4.26 (m, 4H, –OCH_2–), 3.94 (m, 4H, –$CH_2CH_2CH_2$–), 3.05 (m, 4H, –CH_2CH_2-CH_2–), 2.16 (m, 1H, Im), 2.09–(–1.72) (m, 35H); ^{13}C NMR (125 MHz, $CDCl_3$) δ/ppm = 156.20 (C), 155.23 (C), 151.15 (C), 150.05 (C), 149.50 (CH), 148.92 (C), 148.87 (C), 148.34 (C), 148.13 (CH), 146.28 (C), 146.09 (C), 144.68 (C), 137.20 (CH), 136.79 (C), 136.29 (C), 135.65 (CH), 135.57 (CH), 135.48 (CH), 131.74 (CH), 129.60 (CH), 129.43 (CH), 129.29 (CH), 128.46 (CH), 127.84 (CH), 125.12 (CH), 124.90 (CH), 123.92 (CH), 121.41 (CH), 121.33 (CH), 120.37 (C), 119.32 (C), 119.24 (C), 117.59 (CH), 116.87 (CH_2), 116.84 (CH_2), 96.86 (C), 72.17 (CH_2), 70.22 (CH_2), 67.87 (CH_2), 50.58 (CH_2), 50.25 (CH_2), 50.08 (CH_2), 49.91 (CH_2), 47.82 (CH_2), 47.39 (CH_2), 46.53 (CH_2), 45.40 (CH or CH_3), 45.25 (CH or CH_3), 45.01 (CH or CH_3), 44.83 (CH or CH_3), 39.01 (CH or CH_3), 38.75 (CH_2), 36.46 (CH_2), 36.24 (CH_2), 35.64 (CH_2), 35.50 (CH_2), 32.19 (CH or CH_3), 30.67 (C), 30.49 (C), 30.42 (C), 30.29 (C), 30.21 (C), 29.81 (C), 29.63 (CH or CH_3), 29.53 (CH or CH_3), 29.48 (CH or CH_3), 29.45 (CH or CH_3), 29.41 (CH or CH_3), 29.34 (CH or CH_3), 29.09 (CH_2), 28.63 (CH or CH_3), 28.50 (CH or CH_3), 28.25 (CH or CH_3), 28.06 (CH or CH_3), 27.03 (CH or CH_3), 26.91 (CH or CH_3), 26.67 (CH or CH_3), 25.49 (CH_2), 24.09 (CH_2), 23.95 (CH_2), 23.81 (CH_2), 23.75 (CH_2), 23.07 (CH_2), 21.95 (CH or CH_3), 21.91 (CH or CH_3), 21.60 (CH or CH_3), 21.34 (CH or CH_3), 21.28 (CH or CH_3), 16.11 (CH or CH_3), 15.78 (CH or CH_3).

Dimer of Zn porphyrin═Re complex dyad ([Im^{IS}-ZnP-Ph-5Bpy═Re]$_2$, ReDRe). In a 200 mL flask, **[Im^{IS}-ZnP-Ph-5Bpy]$_2$** (130 mg, 0.12 mmol), $Re(CO)_5Br$ (46 mg, 0.11 mmol), and toluene (135 mL) were placed. The mixture was heated to 90 °C and stirred for 2 days. Pyridine (2 mL) was added to the resulting solution and the solvent was evaporated to dryness. The residue was purified with a flush silica gel column (eluent: $CHCl_3$ → $CHCl_3$/acetone = 20/1). The collected fractions were evaporated to dryness, giving the titular compound as a purple solid (120 mg, 72% yield). TLC (silica gel, $CHCl_3$/acetone = 10/1) R_f = 0.5; HPLC (GPC, pyridine, 1.0 mL min^{-1}) RT = 23.4 min; MALDI-TOF-mass (dithranol) *m*/*z* $[M + H]^+$ 1465.4329, calcd for $[C_{72}H_{81}BrN_8O_5ReZn]^+$ 1465.4329; ^{1}H NMR (500 MHz, $CDCl_3$) δ/ppm = 9.69 (m, 3H, β-pyrrole and bpy 6), 9.17 (d, *J* = 5.6 Hz, 1H, bpy 6′), 9.07 (m, 2H, β-pyrrole), 8.96 (m, 2H, β-pyrrole), 8.90 (m, 1H, phenylene), 8.53 (q, *J* = 7.7 Hz, 1H, bpy 3), 8.35 (m, 1H, bpy 3′), 8.27 (m, 2H, phenylene and bpy 4), 8.18 (m, 1H, phenylene), 8.06 (m, 2H, phenylene and bpy 4′), 7.57 (t, *J* = 6.6 Hz, 1H, bpy 5′), 6.21 (m, 2H, –CH═), 5.58 (s, 1H, Im), 5.54 (m, 2H, ═CH_2), 5.44 (m, 2H, β-pyrrole), 5.36 (m, 2H, ═CH_2), 5.25 (m, 4H, –$CH_2CH_2CH_2$–), 4.25 (m, 4H, –OCH_2–), 3.94 (m, 4H, –CH_2CH_2-CH_2–), 3.05 (m, 4H, –$CH_2CH_2CH_2$–), 2.13 (m, 1H, Im), 2.09–(–1.77) (m, 35H); ^{13}C NMR (125 MHz, $CDCl_3$) δ/ppm = 197.17 (CO), 196.88 (CO), 189.20 (CO), 155.80 (C), 153.91 (C), 153.52 (CH), 151.86 (CH), 151.20 (C), 150.25 (C), 148.65 (C), 148.34 (C), 146.61 (C), 145.97 (C), 140.79 (C), 139.00 (CH), 137.04 (CH), 135.99 (CH), 135.88 (CH), 135.43 (CH), 133.18 (C), 131.64 (CH), 131.51 (CH), 129.60 (C), 129.59 (CH), 129.40 (CH), 128.75 (CH), 127.91 (CH), 127.00 (CH), 125.40 (CH), 125.15 (CH), 123.42 (CH), 123.19 (CH), 121.26 (CH), 119.47 (C), 116.94 (CH_2), 97.08 (C), 72.19 (CH_2), 70.17 (CH_2), 67.85 (CH_2), 50.58 (CH_2), 50.24 (CH_2), 50.25 (CH_2), 49.88 (CH_2), 47.84 (CH_2), 47.39 (CH_2), 46.53 (CH_2), 45.24 (CH_3), 45.04 (CH_3), 44.84 (CH_3), 38.78 (CH_2), 36.49 (CH_2), 36.23 (CH_2), 35.62 (CH_2), 35.49 (CH_2), 32.20 (CH_2), 30.65 (C), 30.49 (C), 30.43 (C), 30.23 (C), 29.80 (C), 29.63 (CH_2), 29.45 (CH or CH_3), 29.40 (CH or CH_3), 29.34 (CH or CH_3), 29.08 (C), 28.61 (CH or CH_3), 28.48 (CH or CH_3), 28.22 (CH or CH_3), 28.04 (CH or CH_3), 26.84 (CH or CH_3), 26.61 (CH or CH_3), 25.48 (CH_2), 24.06 (CH_2), 23.94 (CH_2), 23.80 (CH_2), 23.07 (CH_2), 21.94 (CH or CH_3), 21.61 (CH or CH_3), 21.29 (CH or CH_3), 16.09 (CH or CH_3), 15.75 (CH or CH_3); FT-IR (KBr) ν_{CO} = 1900, 1920, 2022 cm^{-1}.

Covalently linked dimers, *C*-[Im^{IS}-ZnP-Ph-5Bpy═Re]$_2$ (ReD′Re) and *C*-[Im^{Me}-ZnP-PhCH$_3$][Im^{IS}-ZnP-Ph-5Bpy═Re] (ReD′). In a test tube, two kinds of noncovalently linked dimers, **[Im^{IS}-ZnP-Ph-5Bpy═Re]$_2$** (70 mg, 0.048 mmol) and **[Im^{Me}-ZnP-PhCH$_3$]$_2$** (35 mg, 0.048 mmol), were placed. Pyridine (6 mL) was added to it and the dimers were dissociated to the corresponding monomers. The solvent was evaporated to dryness under reduced pressure and the residue was dried *in vacuo* at 40 °C for 2 h. The solid was dissolved in $CHCl_3$ (25 mL) and the solution was degassed by freeze–thaw cycles and purged with Ar gas. The Grubbs catalyst (1st generation, 1.3 mg, and 0.0016 mmol) was added to it, and the reaction mixture was stirred at rt under an Ar atmosphere. The reaction progress was monitored with UV–vis absorption spectra in pyridine. The reaction was completed by gradually adding the Grubbs catalyst (total 18 mg, 0.022 mmol). The resulting solution was evaporated to dryness, and the residue was analyzed with gel permeation chromatography (GPC; two TSK G2500H$_{HR}$ and one TSK G2000H$_{HR}$ columns) using pyridine as the eluent. The products of **ReD′Re** and **ReD′** were separated with preparative recycle GPC (one preparative TSK G2500H$_{HR}$ and one preparative TSK G2000H$_{HR}$ columns) using pyridine as the eluent. The second fraction was collected and the solvent was evaporated to dryness, giving a purple solid (16 mg, 12% yield) as **ReD′Re:** HPLC (GPC, pyridine, 1.0 mL min^{-1}) RT = 21.2 min; MALDI-TOF-mass (DCTB) *m*/*z* $[M + H]^+$ 2880.7907, calcd for $[C_{140}H_{153}Br_2N_{16}O_{10}Re_2Zn_2]^+$ 2880.7910 (peak); ^{1}H NMR (500 MHz, $CDCl_3$) δ/ppm = 9.67 (m, 2H, bpy 6), 9.60 (m, 4H, β-pyrrole), 9.16 (m, 2H,bpy 6′), 9.05 (m, 8H, β-pyrrole), 8.92 (m, 2H, phenylene), 8.54 (m, 2H, bpy 4), 8.31 (m, 4H, bpy 3 and bpy 3′), 8.27 (m, 2H, phenylene), 8.20 (m, 2H, phenylene), 8.06 (m, 4H, phenylene and bpy 4′), 7.58 (m, 2H, bpy 5′), 6.46 (s, 2.6H, –CH═ (*E* form)), 6.11 (s, 1.4H, –CH═ (*Z* form)), 5.56 (s, 2H, Im), 5.42 (m, 8H, β-pyrrole and –CH_2CH_2-CH_2–), 5.15 (m, 4H, –$CH_2CH_2CH_2$–), 4.69 (m, 2.8H, –OCH_2-(*Z* form)), 4.44 (m, 5.2H, –OCH_2-(*E* form)), 4.21 (m, 7H,

© 2022 The Author(s). Published by the Royal Society of Chemistry

Open Access Article. Published on 03 augusta 2022. Downloaded on 20.10.2025 1:09:44.
This article is licensed under a Creative Commons Attribution-NonCommercial 3.0 Unported Licence.

–$CH_2CH_2CH_2$–), 3.95 (m, 1H, –$CH_2CH_2CH_2$–), 3.29 (m, 1H, –$CH_2CH_2CH_2$–), 3.13 (m, 3H, –$CH_2CH_2CH_2$–), 3.00 (m, 4H, –$CH_2CH_2CH_2$–), 2.12 (m, 2H, Im), 2.07–(–1.33) (m, 70H); ^{13}C NMR (125 MHz, $CDCl_3$) δ/ppm = 197.53 (CO), 197.23 (CO), 197.14 (CO), 196.86 (CO), 189.79 (CO), 189.19 (CO), 155.82 (C), 153.93 (C), 153.51 (CH), 153.40 (CH), 151.85 (C), 150.91 (C), 150.13 (C), 148.38 (C), 146.54 (C), 140.84 (C), 140.78 (C), 139.10 (CH), 138.98 (CH), 137.10 (CH), 137.05 (CH), 135.93 (CH), 135.84 (CH), 133.23 (C), 131.58 (CH), 129.60 (CH), 128.32 (CH), 127.88 (CH), 127.05 (CH), 125.38 (CH), 125.16 (CH), 123.43 (CH), 123.20 (CH), 119.70 (C), 116.91 (CH_2), 70.80 (CH_2), 70.58 (CH_2), 67.24 (CH_2), 49.93 (CH_2), 47.75 (CH_2), 40.06 (CH_2), 39.01 (CH_2), 32.82 (CH_2), 30.50 (C), 30.30 (C), 29.70 (CH or CH_3), 29.40 (CH or CH_3), 28.25 (CH or CH_3), 27.04 (CH or CH_3), 21.58, (CH or CH_3) 15.97 (CH or CH_3); FT-IR (KBr) ν_{CO} = 1901, 1919, 2021 cm^{-1}. The third fraction of the preparative GPC was collected and the solvent was evaporated to dryness, giving a purple solid (36 mg, 35% yield) as **ReD′**: HPLC (GPC, pyridine, 1.0 mL min^{-1}) RT = 22.1 min; MALDI-TOF-mass (DCTB) *m*/*z* $[M]^+$ 2146.6340, calcd for $[C_{111}H_{114}BrN_{14}O_7ReZn_2]^+$ 2146.6292; ^{1}H NMR (500 MHz, $CDCl_3$) δ/ppm = 9.70–9.62 (m, 2H, β-pyrrole), 9.56 (m, 2H, β-pyrrole), 9.20 (m, 1H, bpy 6), 9.15 (m, 2H, β-pyrrole), 9.08 (m, 4H, β-pyrrole), 8.90 (m, 3H, β-pyrrole and bpy 6′), 8.64 (m, 1H, bpy 3), 8.50 (brs, 2H, phenylene and bpy 3′), 8.18 (m, 1H, phenylene), 8.03 (m, 1H, phenylene), 7.80 (m, 1H, bpy 4), 7.76–7.60 (m, 5H, phenylene and bpy 4′), 7.36 (m, 2H, bpy 5′), 7.25 (brs, 1H, phenylene), 6.49 (s, 2.75H, –CH= (*E* form)), 6.14 (s, 1.25H, –CH= (*Z* form)), 5.57 (m, 3H, β-pyrrole and Im), 5.51 (m, 2H, β-pyrrole), 5.41 (m, 1H, Im), 5.15 (m, 8H, –$CH_2CH_2CH_2$–), 4.70 (m, 2.5H, –OCH_2–(*Z* form)), 4.45 (m, 5.5H, –OCH_2–(*E* form)), 4.28–4.21 (m, 8H, –$CH_2CH_2CH_2$–), 3.33–3.034 (m, 8H, –$CH_2CH_2CH_2$–), 2.85 (s, 3H, CH_3), 2.16 (m, 1H, Im), 1.94 (m, 1H, Im), 1.64 (m, 3H, CH_3), 2.09–(–1.77) (m, 35H); ^{13}C NMR (125 MHz, $CDCl_3$) δ/ppm = 197.36 (CO), 197.16 (CO), 197.00 (CO), 196.80 (CO), 189.60 (CO), 188.98 (CO), 155.25 (C), 153.04 (CH), 151.05 (CH), 150.88 (CH), 150.21 (C), 150.10 (C), 149.81 (CH), 149.27 (C), 149.25 (C), 148.42 (C), 148.16 (C), 146.14 (C), 146.06 (C), 141.16 (C), 138.94 (CH), 138.85 (CH), 137.07 (C), 136.08 (CH), 135.90 (CH), 135.46 (CH), 134.82 (CH), 134.61 (CH), 132.84 (C), 132.50 (CH), 132.40 (CH), 131.47 (CH), 129.97 (CH), 129.62 (CH), 128.29 (CH), 127.87 (CH), 127.64 (CH), 127.35 (CH), 127.26 (CH), 126.54 (CH), 125.06 (CH), 123.82 (CH), 122.77 (CH), 121.47 (CH), 119.81 (C), 118.14 (CH), 116.91 (CH_2), 96.94 (C), 96.47 (C), 72.21 (CH_2), 70.83 (CH_2), 70.60 (CH_2), 67.30 (CH_2), 50.58 (CH_2), 49.90 (CH_2), 47.85 (CH_2), 47.34 (CH_2), 45.02 (CH_3), 40.06 (CH_2), 39.01 (CH_2), 35.63 (CH_2), 32.91 (CH_2), 32.03 (C), 30.50 (C), 30.26 (C), 30.19 (C), 29.81 (CH_2), 29.66 (CH or CH_3), 29.61 (CH or CH_3), 29.50 (CH or CH_3), 29.44 (CH or CH_3), 29.40 (CH or CH_3), 29.35 (CH or CH_3), 28.51 (CH or CH_3), 28.37 (CH or CH_3), 28.28 (CH or CH_3), 28.13 (CH or CH_3), 26.93 (CH or CH_3), 21.94 (CH or CH_3), 21.79 (CH or CH_3), 21.60 (CH or CH_3), 21.29 (CH or CH_3), 15.80 (CH or CH_3); FT-IR (KBr) ν_{CO} = 1900, 1920, 2022 cm^{-1}.

Covalently linked dimer, *C*-[Im^{IS}-ZnP-Ph-5Bpy=Re]$_2$ (ReD′Re). The noncovalently linked dimer, **[Im^{IS}-ZnP-Ph-5Bpy=Re]$_2$**, (4.8 mg, 0.0033 mmol) and CH_2Cl_2 (5.0 mL) were placed in a 20 mL Schlenk tube and the solution was degassed by freeze–thaw cycles. Grubbs catalyst (1st generation, 0.22 mg, and 0.00027 mmol) was added to it, and the reaction mixture was stirred at rt under an Ar atmosphere. The reaction progress was monitored with UV-vis absorption spectra in pyridine. After being stirred overnight, the resulting solution was evaporated to dryness. The residue was purified with a flush silica gel column (eluent: $CHCl_3$ → $CHCl_3$/acetone = 10/1). The collected solution was evaporated to dryness, giving a purple solid (3.8 mg, 87% yield).

Quenching experiments. The Stern–Volmer relationship (eqn (1)) was obtained from the plots of the relative emission peak area (Φ_0/Φ) *versus* the concentration of BIH:

$$\Phi_o/\Phi = 1 + K_{sv}[BIH] = 1 + k_q\tau[BIH] \quad (1)$$

where Φ_0 and F represent the emission peak area in the absence and presence of BIH, respectively, and K_{sv}, k_q, and τ are the Stern–Volmer constant, the quenching rate constant, and the emission lifetime, respectively. The DMA solutions containing the porphyrins in square quartz cells (l = 1.0 cm) were used.

Photocatalytic CO_2 reduction. In glass tubes (8.0 mL, i.d. = 10 mm), 1.0 mL of CO_2-saturated DMA solutions containing BIH was added to 1.0 mL of Ar-saturated DMA solutions containing the photocatalysts, and the reaction solutions were bubbled through septum caps with CO_2 gas for 20 min. Photo-irradiations to determine the TON were carried out using a merry-go-round irradiation apparatus (Iris-MG, Cell Systems) equipped with LED lamps at 25 °C. Reaction quantum yields (Φ) were determined with an Asahi Spectra PRA-201 apparatus equipped with a Xe lamp (Asahi Spectra, MAX-350) and calculated according to eqn (2):

$$\Phi = \frac{[CO_2 \text{ reduction products}]}{[\text{incident photons}]} \quad (2)$$

The solutions in 7 mL quartz cubic cells (optical path length: 1.0 cm) were irradiated with light at 420, 450 or 560 nm using bandpass filters. The concentrations of the catalysts were 0.025 mM (420 and 450 nm) and 0.1 mM (560 nm). The gaseous reaction products (CO and H_2) were quantified with a gas chromatography system (GC-2014, Shimadzu Science) equipped with a Shincarbon column (i.d. 3.0 mm × 3.0 m) and a thermal conductivity detector (TCD). The product (formate) in the solutions was analyzed with a capillary electrophoresis system (Otuka Electronics Co. CAPI-3300I).

Author contributions

Y. K. conceived the idea, designed and performed some of the photocatalytic experiments, and wrote the manuscript. R. S. synthesized and characterized the isostearyl-substituted porphyrins, and performed most of the photocatalytic experiments. H. S. synthesized the methyl-substituted porphyrins. A. S. supervised the project, and provided suggestions on the experiments and writing the manuscript.

Conflicts of interest

There are no conflicts to declare.

Open Access Article. Published on 03 augusta 2022. Downloaded on 20.10.2025 1:09:44.
This article is licensed under a Creative Commons Attribution-NonCommercial 3.0 Unported Licence.

Acknowledgements

This work was supported by JSPS KAKENHI Grant Numbers JP19K05677 and JP22H02186. We thank Prof. Akihiko Kudo (Tokyo University of Science) for help with capillary electrophoresis analyses.

References

1 (*a*) T. R. Cook, D. K. Dogutan, S. Y. Reece, Y. Surendranath, T. S. Teets and D. G. Nocera, Solar Energy Supply and Storage for the Legacy and Nonlegacy Worlds, *Chem. Rev.*, 2010, **110**, 6474–6502; (*b*) G. A. Olah, G. K. S. Prakash and A. Goeppert, Anthropogenic Chemical Carbon Cycle for a Sustainable Future, *J. Am. Chem. Soc.*, 2011, **133**, 12881–12898.

2 (*a*) H. Inoue, T. Shimada, Y. Kou, Y. Nabetani, D. Masui, S. Takagi and H. Tachibana, The Water Oxidation Bottleneck in Artificial Photosynthesis: How Can We Get Through It? An Alternative Route Involving a Two-Electron Process, *ChemSusChem*, 2011, **4**, 173–179; (*b*) J.-H. Alstrum-Acevedo, M. K. Brennaman and T. J. Meyer, Chemical Approaches to Artificial Photosynthesis. 2, *Inorg. Chem.*, 2005, **44**, 6802–6827.

3 (*a*) A. W. Roszak, T. D. Howard, J. Southall, A. T. Gardiner, C. J. Law, N. W. Isaacs and R. J. Cogdell, Crystal Structure of the RC-LH1 Core Complex from *Rhodopseudomonas palustris*, *Science*, 2003, **302**, 1969–1972; (*b*) G. McDermott, S. M. Prince, A. A. Freer, A. M. Hawthornthwaite-Lawless, M. Z. Papiz, R. J. Cogdell and N. W. Isaacs, Crystal Structure of an Integral Membrane Light-Harvesting Complex from Photosynthetic Bacteria, *Nature*, 1995, **374**, 517–521.

4 (*a*) R. E. Blankenship, *Molecular Mechanisms of Photosynthesis*, Blackwell, Oxford, 2001; (*b*) J. Deisenhofer, O. Epp, K. Miki, R. Huber and H. Michel, Structure of the Protein Subunits in the Photosynthetic Reaction Centre of *Rhodopseudomonas viridis* at 3Å Resolution, *Nature*, 1985, **318**, 618–624.

5 Y. Kobuke and H. Miyaji, Supramolecular Organization of Imidazolyl-Porphyrin to a Slipped Cofacial Dimer, *J. Am. Chem. Soc.*, 1994, **116**, 4111–4112.

6 (*a*) F. Ito, Y. Ishibashi, S. R. Khan, H. Miyasaka, K. Kameyama, M. Morisue, A. Satake, K. Ogawa and Y. Kobuke, Photoinduced Electron Transfer and Excitation Energy Transfer in Directly Linked Zinc Porphyrin/Zinc Phthalocyanine Composite, *J. Phys. Chem. A*, 2006, **110**, 12734–12742; (*b*) H. Ozeki, A. Nomoto, K. Ogawa, Y. Kobuke, M. Murakami, K. Hosoda, M. Ohtani, S. Nakashima, H. Miyasaka and T. Okada, Role of the Special Pair in the Charge-Separating Event in Photosynthesis, *Chem. – Eur. J.*, 2004, **10**, 6393–6401.

7 K. Yoneyama, R. Suzuki, Y. Kuramochi and A. Satake, A Candidate for Multitopic Probes for Ligand Discovery in Dynamic Combinatorial Chemistry, *Molecules*, 2019, **24**, 2166.

8 H. Nakagawa, K. Ogawa, A. Satake and Y. Kobuke, A Supramolecular Photosynthetic Triad of Slipped Cofacial Porphyrin Dimer, Ferrocene, and Fullerene, *Chem. Commun.*, 2006, 1560–1562.

9 (*a*) Y. Kuramochi, A. Satake, A. S. D. Sandanayaka, Y. Araki, O. Ito and Y. Kobuke, Fullerene- and Pyromellitdiimide-Appended Tripodal Ligands Embedded in Light-Harvesting Porphyrin Macrorings, *Inorg. Chem.*, 2011, **50**, 10249–10258; (*b*) A. Satake, S. Azuma, Y. Kuramochi, S. Hirota and Y. Kobuke, Supramolecular Organization of Light-Harvesting Porphyrin Macrorings, *Chem. – Eur. J.*, 2011, **17**, 855–865; (*c*) Y. Kuramochi, A. S. D. Sandanayaka, A. Satake, Y. Araki, K. Ogawa, O. Ito and Y. Kobuke, Energy Transfer Followed by Electron Transfer in a Porphyrin Macrocycle and Central Acceptor Ligand: A Model for a Photosynthetic Composite of the Light-Harvesting Complex and Reaction Center, *Chem. – Eur. J.*, 2009, **15**, 2317–2327; (*d*) N. Nagata, Y. Kuramochi and Y. Kobuke, Energy Transfer among Light-Harvesting Macrorings Incorporated into a Bilayer Membrane, *J. Am. Chem. Soc.*, 2009, **131**, 10–11; (*e*) Y. Kuramochi, A. Satake, M. Itou, K. Ogawa, Y. Araki, O. Ito and Y. Kobuke, Light-Harvesting Supramolecular Porphyrin Macrocycle Accommodating a Fullerene−Tripodal Ligand, *Chem. – Eur. J.*, 2008, **14**, 2827–2841; (*f*) Y. Kuramochi, A. Satake and Y. Kobuke, Light-Harvesting Macroring Accommodating a Tetrapodal Ligand Based on Complementary and Cooperative Coordinations, *J. Am. Chem. Soc.*, 2004, **126**, 8668–8669.

10 (*a*) F. Hajjaj, Z. S. Yoon, M.-C. Yoon, J. Park, A. Satake, D. Kim and Y. Kobuke, Assemblies of Supramolecular Porphyrin Dimers in Pentagonal and Hexagonal Arrays Exhibiting Light-Harvesting Antenna Function, *J. Am. Chem. Soc.*, 2006, **128**, 4612–4623; (*b*) R. Takahashi and Y. Kobuke, Hexameric Macroring of Gable-Porphyrins as a Light-Harvesting Antenna Mimic, *J. Am. Chem. Soc.*, 2003, **125**, 2372–2373.

11 S. Morikawa, C. Ikeda, K. Ogawa and Y. Kobuke, Two-Dimensional Porphyrin Array Assembled by Self-Coordination, *Lett. Org. Chem.*, 2004, **1**, 6–11.

12 (*a*) J. E. Raymond, A. Bhaskar, T. Goodson III, N. Makiuchi, K. Ogawa and Y. Kobuke, Synthesis and Two-Photon Absorption Enhancement of Porphyrin Macrocycles, *J. Am. Chem. Soc.*, 2008, **130**, 17212–17213; (*b*) K. Ogawa, A. Ohashi, Y. Kobuke, K. Kamada and K. Ohta, Strong Two-Photon Absorption of Self-Assembled Butadiyne-Linked Bisporphyrin, *J. Am. Chem. Soc.*, 2003, **125**, 13356–13357; (*c*) K. Ogawa, T. Zhang, K. Yoshihara and Y. Kobuke, Large Third-Order Optical Nonlinearity of Self-Assembled Porphyrin Oligomers, *J. Am. Chem. Soc.*, 2002, **124**, 22–23.

13 (*a*) M. Morisue, D. Kalita, N. Haruta and Y. Kobuke, Fine-Tuning of a Ferrocene|porphyrin|ITO Redox Cascade for Efficient Sequential Electron Transfer Commenced by an S_2 Photoexcited Special Pair Mimic, *Chem. Commun.*, 2007, 2348–2350; (*b*) M. Morisue, N. Haruta, D. Kalita and Y. Kobuke, Efficient Charge Injection from the S_2 Photoexcited State of Special-Pair Mimic Porphyrin

© 2022 The Author(s). Published by the Royal Society of Chemistry

Open Access Article. Published on 03 augusta 2022. Downloaded on 20.10.2025 1:09:44.
This article is licensed under a Creative Commons Attribution-NonCommercial 3.0 Unported Licence.

Assemblies Anchored on a Titanium-Modified ITO Anode, *Chem. – Eur. J.*, 2006, **12**, 8123–8135.

14 (*a*) M. Sugimoto, Y. Kuramochi and A. Satake, Measurement of Solvation Ability of Solvents by Porphyrin-Based Solvation/Desolvation Indicators, *ACS Omega*, 2020, **5**, 6045–6050; (*b*) A. Satake, Y. Suzuki, M. Sugimoto and Y. Kuramochi, Mechanistic Study of the Solvent-Dependent Formation of Extended and Stacked Supramolecular Polymers Composed of Bis(imidazolylporphyrinatozinc) Molecules, *Chem. – Eur. J.*, 2020, **26**, 669–684; (*c*) A. Satake, Y. Suzuki, M. Sugimoto, T. Shimazaki, H. Ishii and Y. Kuramochi, A Solvation/Desolvation Indicator Based on van der Waals Interactions between Solvents and Porphyrins, *Chem. – Eur. J.*, 2018, **24**, 14733–14741.

15 (*a*) K. Rybicka-Jasinska, W. Shan, K. Zawada, K. M. Kadish and D. Gryko, Porphyrins as Photoredox Catalysts: Experimental and Theoretical Studies, *J. Am. Chem. Soc.*, 2016, **138**, 15451–15458; (*b*) S. Shanmugam, J. Xu and C. Boyer, Exploiting Metalloporphyrins for Selective Living Radical Polymerization Tunable over Visible Wavelengths, *J. Am. Chem. Soc.*, 2015, **137**, 9174–9185; (*c*) T. Lazarides, I. V. Sazanovich, A. J. Simaan, M. C. Kafentzi, M. Delor, Y. Mekmouche, B. Faure, M. Reglier, J. A. Weinstein, A. G. Coutsolelos and T. Tron, Visible Light-Driven O_2 Reduction by a Porphyrin–Laccase System, *J. Am. Chem. Soc.*, 2013, **135**, 3095–3103; (*d*) R. Miyatani and Y. Amao, Photochemical Synthesis of Formic Acid from CO_2 with Formate Dehydrogenase and Water-Soluble Zinc Porphyrin, *J. Mol. Catal. B: Enzym.*, 2004, **27**, 121–125.

16 (*a*) P. Lang, M. Pfrunder, G. Quach, B. Braun-Cula, E. G. Moore and M. Schwalbe, Sensitized Photochemical CO_2 Reduction by Hetero–Pacman Compounds Linking a Re^{I} Tricarbonyl with a Porphyrin Unit, *Chem. – Eur. J.*, 2019, **25**, 4509–4519; (*b*) C. Matlachowski, B. Braun, S. Tschierlei and M. Schwalbe, Photochemical CO_2 Reduction Catalyzed by Phenanthroline Extended Tetramesityl Porphyrin Complexes Linked with a Rhenium(I) Tricarbonyl Unit, *Inorg. Chem.*, 2015, **54**, 10351–10360; (*c*) C. D. Windle, M. W. George, R. N. Perutz, P. A. Summers, X. Z. Sun and A. C. Whitwood, Comparison of Rhenium–Porphyrin Dyads for CO_2 Photoreduction: Photocatalytic Studies and Charge Separation Dynamics Studied by Time-Resolved IR Spectroscopy, *Chem. Sci.*, 2015, **6**, 6847–6864; (*d*) C. D. Windle, M. V. Campian, A.-K. Duhme-Klair, E. A. Gibson, R. N. Perutz and J. Schneider, CO_2 Photoreduction with Long-Wavelength Light: Dyads and Monomers of Zinc Porphyrin and Rhenium Bipyridine, *Chem. Commun.*, 2012, **48**, 8189–8191; (*e*) K. Kiyosawa, N. Shiraishi, T. Shimada, D. Masui, H. Tachibana, S. Takagi, O. Ishitani, D. A. Tryk and H. Inoue, Electron Transfer from the Porphyrin S_2 State in a Zinc Porphyrin-Rhenium Bipyridyl Dyad having Carbon Dioxide Reduction Activity, *J. Phys. Chem. C*, 2009, **113**, 11667–11673.

17 (*a*) S. H. Choi, C. H. Kim, J.-O. Baeg, H. J. Son, C. Pac and S. O. Kang, Collisional Electron Transfer Route between Homogeneous Porphyrin Dye and Catalytic TiO_2/Re(I) Particles for CO_2 Reduction, *ACS Appl. Energy Mater.*, 2020, **3**, 11581–11596; (*b*) D.-I. Won, J.-S. Lee, Q. Ba, Y.-J. Cho, H.-Y. Cheong, S. Choi, C. H. Kim, H.-J. Son, C. Pac and S. O. Kang, Development of a Lower Energy Photosensitizer for Photocatalytic CO_2 Reduction: Modification of Porphyrin Dye in Hybrid Catalyst System, *ACS Catal.*, 2018, **8**, 1018–1030.

18 (*a*) Y. Kuramochi and A. Satake, Photocatalytic CO_2 Reductions Catalyzed by *meso*-(1,10-Phenanthrolin-2-yl)-Porphyrins Having a Rhenium(I) Tricarbonyl Complex, *Chem. – Eur. J.*, 2020, **26**, 16365–16373; (*b*) Y. Kuramochi and Y. Fujisawa, A. Satake, Photocatalytic CO_2 Reduction Mediated by Electron Transfer *via* the Excited Triplet State of Zn(II) Porphyrin, *J. Am. Chem. Soc.*, 2020, **142**, 705–709.

19 A. Satake and Y. Kobuke, Artificial Photosynthetic Systems: Assemblies of Slipped Cofacial Porphyrins and Phthalocyanines Showing Strong Electronic Coupling, *Org. Biomol. Chem.*, 2007, **5**, 1679–1691.

20 A. Ohashi, A. Satake and Y. Kobuke, Covalent Linking of Coordination-Organized Slipped Cofacial Porphyrin Dimers, *Bull. Chem. Soc. Jpn.*, 2004, **77**, 365–374.

21 We used 2nd generation Grubbs catalyst, benzylidene[1,3-bis(2,4,6-trimethylphenyl)-2-imidazolidinylidene] dichloro(tricyclohexylphosphine)ruthenium, instead of 1st generation Grubbs catalyst but it did not improve the reaction progress. It was reported that 2nd generation Grubbs catalyst gave benzylidene-substituted byproducts in the metathesis reaction for the porphyrin dimer. See:C. Ikeda, A. Satake and Y. Kobuke, Proofs of Macrocyclization of Gable Porphyrins as Mimics of Photosynthetic Light-Harvesting Complexes, *Org. Lett.*, 2003, **5**, 4935–4938.

22 (*a*) S. Hitosugi, D. Tanimoto, W. Nakanishi and H. Isobe, A Facile Chromatographic Method for Purification of Pinacol Boronic Esters, *Chem. Lett.*, 2012, **41**, 972–973; (*b*) A. Lützen, M. Hapke, H. Staats and J. Bunzen, Synthesis of Differently Disubstituted 2,2'-Bipyridines by a Modified Negishi Cross-Coupling Reaction, *Eur. J. Org. Chem.*, 2003, 3948–3957.

23 S. Sato, T. Morimoto and O. Ishitani, Photochemical Synthesis of *mer*-[Re(bpy)$(CO)_3$Cl], *Inorg. Chem.*, 2007, **46**, 9051–9053.

24 O. Shoji, S. Okada, A. Satake and Y. Kobuke, Coordination Assembled Rings of Ferrocene-Bridged Trisporphyrin with Flexible Hinge-like Motion: Selective Dimer Ring Formation, Its Transformation to Larger Rings, and Vice Versa, *J. Am. Chem. Soc.*, 2005, **127**, 2201–2210.

25 Y. Kuramochi, M. Kamiya and H. Ishida, Photocatalytic CO_2 Reduction in *N,N*-Dimethylacetamide/Water as an Alternative Solvent System, *Inorg. Chem.*, 2014, **53**, 3326–3332.

26 Y. Kuramochi, Y. Kawakami and A. Satake, Synthesis and Photophysical Properties of Porphyrin Macrorings Composed of Freebase Porphyrins and Slipped-Cofacial Zinc Porphyrin Dimers, *Inorg. Chem.*, 2017, **56**, 11008–11018.

27 Y. Kuramochi, S. Hashimoto, Y. Kawakami, M. S. Asano and A. Satake, Visualization of Nonemissive Triplet Species of

Open Access Article. Published on 03 augusta 2022. Downloaded on 20.10.2025 1:09:44.
This article is licensed under a Creative Commons Attribution-NonCommercial 3.0 Unported Licence.

Zn(II) Porphyrins through Cu(II) Porphyrin Emission *via* the Reservoir Mechanism in a Porphyrin Macroring, *Photochem. Photobiol. Sci.*, 2018, **17**, 883–888.

28 Y. Kuramochi, O. Ishitani and H. Ishida, Reaction Mechanisms of Catalytic Photochemical CO_2 Reduction using Re(I) and Ru(II) Complexes, *Coord. Chem. Rev.*, 2018, **373**, 333–356.

29 J. M. Smieja, E. E. Benson, B. Kumar, K. A. Grice, C. S. Seu, A. J. M. Miller, J. M. Mayer and C. P. Kubiak, Kinetic and Structural Studies, Origins of Selectivity, and Interfacial Charge Transfer in the Artificial Photosynthesis of CO, *Proc. Natl. Acad. Sci. U. S. A.*, 2012, **109**, 15646–15650.

30 (*a*) T. Nakajima, Y. Tamaki, K. Ueno, E. Kato, T. Nishikawa, K. Ohkubo, Y. Yamazaki, T. Morimoto and O. Ishitani, Photocatalytic Reduction of Low Concentration of CO_2, *J. Am. Chem. Soc.*, 2016, **138**, 13818–13821; (*b*) T. Morimoto, T. Nakajima, S. Sawa, R. Nakanishi, D. Imori and O. Ishitani, CO_2 Capture by a Rhenium(I) Complex with the Aid of Triethanolamine, *J. Am. Chem. Soc.*, 2013, **135**, 16825–16828.

31 H. W. Whitlock and M. Y. Oester, Chemistry of Porphyrins. IV. Behavior of Di- and Tetrahydroporphyrins under Alkaline Conditions. Direct Observation of the Chlorin-Phlorin Equilibrium, *J. Am. Chem. Soc.*, 1973, **95**, 5738–5741.

32 (*a*) H. Yamaguchi, A. Soeta, H. Toeda and K. Itoh, Raman Scattering Study on Electrochemical Reduction Products of Magnesium, Zinc and Copper Tetraphenylporphines, *J. Electroanal. Chem. Interfacial Electrochem.*, 1983, **159**, 347–359; (*b*) J. G. Lanese and G. S. Wilson, Electrochemical Studies of Zinc Tetraphenylporphin, *J. Electrochem. Soc.*, 1972, **119**, 1039–1043; (*c*) G. L. Closs and L. E. Closs, Negative Ions of Porphin Metal Complexes, *J. Am. Chem. Soc.*, 1963, **85**, 818–819.

33 Y. Harel and J. Manassen, Photoreduction of Tetraphenylporphyrins by Amines in the Visible. Photochemical Syntheses of Reduced Tetraphenylporphyrins and the Mechanism of Photoreduction, *J. Am. Chem. Soc.*, 1978, **100**, 6228–6234.

34 Y. Tamaki, T. Morimoto, K. Koike and O. Ishitani, Photocatalytic CO_2 Reduction with High Turnover Frequency and Selectivity of Formic Acid Formation using Ru(II) Multinuclear Complexes, *Proc. Natl. Acad. Sci. U.S.A.*, 2012, **109**, 15673–15678.

35 (*a*) J. Rohacova and O. Ishitani, Rhenium(I) Trinuclear Rings as Highly Efficient Redox Photosensitizers for Photocatalytic CO_2 Reduction, *Chem. Sci.*, 2016, **7**, 6728–6739; (*b*) V. S. Thoi, N. Kornienko, C. G. Margarit, P. Yang and C. J. Chang, Visible-Light Photoredox Catalysis: Selective Reduction of Carbon Dioxide to Carbon Monoxide by a Nickel N-Heterocyclic Carbene–Isoquinoline Complex, *J. Am. Chem. Soc.*, 2013, **135**, 14413–14424; (*c*) Y. Tamaki, K. Watanabe, K. Koike, H. Inoue, T. Morimoto and O. Ishitani, Development of Highly Efficient Supramolecular CO_2 Reduction Photocatalysts with High Turnover Frequency and Durability, *Faraday Discuss.*, 2012, **155**, 115–127; (*d*) H. Hori, F. P. A. Johnson, K. Koike, O. Ishitani and T. Ibusuki, Efficient Photocatalytic CO_2 Reduction using $[Re(bpy)(CO)_3\{P(OEt)_3\}]^+$, *J. Photochem. Photobiol., A*, 1996, **96**, 171–174.

36 H. Takeda, K. Koike, H. Inoue and O. Ishitani, Development of an Efficient Photocatalytic System for CO_2 Reduction Using Rhenium(I) Complexes Based on Mechanistic Studies, *J. Am. Chem. Soc.*, 2008, **130**, 2023–2031.

37 K. M. Kadish, L. R. Shiue, R. K. Rhodes and L. A. Bottomley, Reactions of Metalloporphyrin .pi. Radicals. 1. Complexation of Zinc Tetraphenylporphyrin Cation and Anion Radicals with Nitrogenous Bases, *Inorg. Chem.*, 1981, **20**, 1274–1277.

38 K. Kamogawa, Y. Shimoda, K. Miyata, K. Onda, Y. Yamazaki, Y. Tamaki and O. Ishitani, Mechanistic Study of Photocatalytic CO_2 Reduction using a Ru(II)-Re(I) Supramolecular Photocatalyst, *Chem. Sci.*, 2021, **12**, 9682–9693.

39 (*a*) H. Jing, S. Liu, J. Jiang, V.-P. Tran, J. Rong, P. Wang and J. S. Lindsey, *Meso* Bromination and Derivatization of Synthetic Bacteriochlorins, *New J. Chem.*, 2022, **46**, 5556–5572; (*b*) J. M. Dąbrowski, L. G. Arnaut, M. M. Pereira, C. J. P. Monteiro, K. Urbańska, S. Simões and G. Stochel, New Halogenated Water-Soluble Chlorin and Bacteriochlorin as Photostable PDT Sensitizers: Synthesis, Spectroscopy, Photophysics, and *in vitro* Photosensitizing Efficacy, *ChemMedChem*, 2010, **5**, 1770–1780; (*c*) J. R. McCarthy, J. Bhaumik, N. Merbouh and R. Weissleder, High-yielding Syntheses of Hydrophilic Conjugatable Chlorins and Bacteriochlorins, *Org. Biomol. Chem.*, 2009, **7**, 3430–3436.

40 M. Taniguchi and J. S. Lindsey, Synthetic Chlorins, Possible Surrogates for Chlorophylls, Prepared by Derivatization of Porphyrins, *Chem. Rev.*, 2017, **117**, 344–535.

41 Y. Tamaki, K. Koike, T. Morimoto and O. Ishitani, Substantial Improvement in the Efficiency and Durability of a Photocatalyst for Carbon Dioxide Reduction Using a Benzoimidazole Derivative as an Electron Donor, *J. Catal.*, 2013, **304**, 22–28.

42 Y. Kou, Y. Nabetani, D. Masui, T. Shimada, S. Takagi, H. Tachibana and H. Inoue, Direct Detection of Key Reaction Intermediates in Photochemical CO_2 Reduction Sensitized by a Rhenium Bipyridine Complex, *J. Am. Chem. Soc.*, 2014, **136**, 6021–6030.

43 (*a*) Y. Kou, Y. Nabetani, R. Nakazato, N. V. Pratheesh, T. Sato, S. Nozawa, S. Adachi, H. Tachibana and H. Inoue, Mechanism of the Photoreduction of Carbon Dioxide Catalyzed by the Benchmarking Rhenium Dimethylbipyridine Complexes; Operando Measurements by XAFS and FT-IR, *J. Catal.*, 2022, **405**, 508–519; (*b*) C. D. Windle, E. Pastor, A. Reynal, A. C. Whitwood, Y. Vaynzof, J. R. Durrant, R. N. Perutz and E. Reisner, Improving the Photocatalytic Reduction of CO_2 to CO through Immobilisation of a Molecular Re Catalyst on TiO_2, *Chem.–Eur. J.*, 2015, **21**, 3746–3754.

44 D. Kalita, M. Morisue and Y. Kobuke, Synthesis and Electrochemical Properties of Slipped-Cofacial Porphyrin Dimers of Ferrocene-Functionalized Zn-Imidazolyl-

© 2022 The Author(s). Published by the Royal Society of Chemistry

Open Access Article. Published on 03 augusta 2022. Downloaded on 20.10.2025 1:09:44.
This article is licensed under a Creative Commons Attribution-NonCommercial 3.0 Unported Licence.

Porphyrins as Potential Terminal Electron Donors in Photosynthetic Models, *New J. Chem.*, 2006, **30**, 77–92.

45 (*a*) X.-Q. Zhu, M.-T. Zhang, A. Yu, C.-H. Wang and J.-P. Cheng, Hydride, Hydrogen Atom, Proton, and Electron Transfer Driving Forces of Various Five-Membered Heterocyclic Organic Hydrides and Their Reaction Intermediates in Acetonitrile, *J. Am. Chem. Soc.*, 2008, **130**, 2501–2516; (*b*) E. Hasegawa, T. Seida, N. Chiba, T. Takahashi and H. Ikeda, Contrastive Photoreduction Pathways of Benzophenones Governed by Regiospecific Deprotonation of Imidazoline Radical Cations and Additive Effects, *J. Org. Chem.*, 2005, **70**, 9632–9635.

46 D. J. Quimby and F. R. Longo, Luminescence Studies on Several Tetraarylporphins and Their Zinc Derivatives, *J. Am. Chem. Soc.*, 1975, **97**, 5111–5117.